Title A highly active bacterial actin actuates the polymerization of another isoform essential for swimming motility of *Spiroplasma*

Authors
Daichi Takahashi[1,†], Hana Kiyama[1], Hideaki T. Matsubayashi[2], Ikuko Fujiwara[1,3,*], Makoto Miyata[1,4]

Affiliations
[1]Graduate School of Science, Osaka Metropolitan University, Osaka, Japan
[2]Frontier Research Institute for Interdisciplinary Sciences, Tohoku University, Miyagi, Japan
[3]Department of Materials Science and Bioengineering, Nagaoka University of Technology, Nagaoka, Niigata, Japan
[4]The OMU Advanced Research Center for Natural Science and Technology, Osaka Metropolitan University, Osaka, Japan
[*]Corresponding author: ikukofujiwara@vos.nagaokaut.ac.jp
[†]Current affiliation: Research Institute for Interdisciplinary Science, Okayama University, Okayama, Japan

Abstract

Spiroplasma is a wall-less helical bacterium possessing five isoforms of bacterial actin MreBs (SMreB1–5) for its swimming, speculated to be the sole motility system driven by endogenous bacterial actin proteins. Its detailed molecular mechanism remains elusive due to the lack of soluble constructs of SMreB1 essential for *Spiroplasma* swimming. Here, we isolated soluble SMreB1 of *Spiroplasma eriocheiris* (SpeMreB1) and evaluated its activity. The phosphate release rate and fold changes of polymerization-critical concentrations over the nucleotide states of SpeMreB1 are the highest among the MreB family proteins. SpeMreB1 interacts with polymerized SpeMreB5, another SMreB essential for *Spiroplasma* swimming, and decreases SpeMreB5 filament amount depending on the nucleotide state. A decrease in SpeMreB5 filament amount is independent of SpeMreB1 polymerization, although it is essential for swimming motility. SpeMreB1 binds to negatively charged lipids, regardless of their nucleotide state. These results suggest that SpeMreB1 manages SpeMreB5 filaments to drive *Spiroplasma* swimming.

Introduction

Motility is the ability of an organism to move directionally from one starting point to another using mechanical energy (converted from chemical energy). Because this ability plays an important role in the survival of organisms, such as obtaining nutrients and evading predators, the evolution of motility has been linked to that of organisms (*1*). Most bacterial species use flagellar rotation and/or pili contraction for their motility (*2*). The bacterial cell wall, the peptidoglycan layer, is important for anchoring the motility machinery (*1*). However, because of its conservation within the bacteria kingdom, the peptidoglycan layer is often targeted by natural immunity (*3, 4*). Therefore, the absence of peptidoglycans is likely advantageous to pathogenic bacteria (*1, 5*). Certain peptidoglycan-deficient species have evolved unique motility systems that do not rely on conventional bacterial motility machinery (*1*).

Spiroplasma, a phylogenetically related species of *Mycoplasma*, is a wall-less helical bacterium pathogenic to plants and arthropods. *Spiroplasma* is often considered industrially problematic, as certain species of it exhibit strong pathogenicity to host organisms (*6-9*). *Spiroplasma* has evolved a unique motility system possibly to sustain itself in the host (*1*). *Spiroplasma* swims by propagating its cell helicity switching along the cell axis to generate a propulsive force (*10-12*). A recent study suggested that the swimming motility of *Spiroplasma* is related to its pathogenicity (*6*), as does the motility of other pathogenic organisms (*1*). Each *Spiroplasma* species possesses five classes of bacterial actin proteins MreB (SMreB1–5), which are thought to contribute to swimming motility (*13-17*). Although MreB is conserved in many bacteria, especially those with elongated cell shapes and cell walls, its role is related to cell shape maintenance rather than directly driving motility (*18*). In walled-bacteria, MreB filaments bind to the cell membrane and support the formation and localization of a peptidoglycan synthesis complex (elongasome complex) (*19, 20*). MreB filaments move along the cell membrane in a direction perpendicular to the major cell axis. As intracellular MreB dynamics are driven by the peptidoglycan synthesis of the elongasome complex rather than by the polymerization dynamics of MreB itself, MreB is believed to be passively involved in the elongasome (*21, 22*). The passive nature of MreB is also suggested by its small conformational change upon polymerization compared to other actin superfamily proteins (*23*). It is an open question how a dynamic machinery system like *Spiroplasma* swimming could be driven by MreB family proteins, which are supposed to be static in cells.

Because of its importance in pathogenicity and the evolutionary interest, *Spiroplasma* swimming has been studied from several perspectives, including cellular and molecular biology (*24*). A recent study using JCVI-syn3B, a minimal synthetic bacterium, revealed that a combination of SMreB5 and either the phylogenetically related SMreB1 or SMreB4 is essential for *Spiroplasma* swimming (*14*). SMreB5 has been studied biochemically and structurally, and the following properties have been reported (*16, 25-27*): SMreB5 possesses ATPase and polymerization activities similar to eukaryotic actin; SMreB5 forms asymmetric sheets, including antiparallel filaments common to the studied MreBs and parallelly oriented protofilaments; SMreB5 binds to a negatively charged membrane mimicking the *Spiroplasma* cell via its positively charged and unstructured C-terminal tail; and SMreB5 forms bundles depending on its ATPase activity and surface charge. However, SMreB1 and SMreB4 have not been studied because of a lack of soluble constructs (*26*).

In the present study, we solubilized SMreB1 and analyzed it using biochemical techniques. SMreB1 of the crustacean pathogen *Spiroplama eriocheiris* (*7*) (SpeMreB1) was fused with ProteinS (PrS), which is a spore surface protein of a soil bacterium *Myxococcus xanthus* and has also been reported as a solubilization tag (*28*). Soluble SpeMreB1 was investigated for its activity, crosstalk with SpeMreB5, and its membrane-binding ability. Based on these analyses, we discuss the functions of SpeMreB1.

Results

Preparation of PrS-fused soluble SpeMreB1

As previously reported (*26*), neither the 6×His-tag fused SpeMreB1 nor SpeMreB4 was soluble (Fig. S1A). This was also the case for SMreB1 and SMreB4, which were derived from different *Spiroplasma* species (Fig. S1B–C, Supplementary data 2). We co-expressed SpeMreB4 and SpeMreB5 because the genes for expressing them are coded in tandem in the genomes of many *Spiroplasma* species (*17*, *29*). However, this approach did not solve the insolubility problem of SpeMreB4 (Fig. S1D). Therefore, we used a solubilization tag for SpeMreB1 and SpeMreB4. We fused two consecutive ProteinS (PrS) molecules at the N-termini of SpeMreB1 and SpeMreB4 (PrS-SpeMreB1 and PrS-SpeMreB4, respectively) and a 6×His-tag at their C-termini (Fig. 1A, Supplementary data 1) and successfully purified them using Ni^{2+}-NTA affinity chromatography and gel filtration (Fig. S1E). During gel filtration, all PrS-SpeMreB4 molecules were eluted in the void fraction where the molecular size exceeded the upper separation limit of the column, indicating that PrS-SpeMreB4 formed oligomers. In contrast, PrS-SpeMreB1 was eluted in both the void and monomeric fractions (Fig. 1B). The oligomer formation of PrS-SpeMreB1 and PrS-SpeMreB4 was probably not caused by the soluble aggregation of PrS, as is reported with other solubilization tags (*30*) because the PrS tag itself was eluted in the monomeric fraction even at a high concentration for the purification and the following assays (50 μM) (Fig. S2A).

Polymerization of SpeMreB1 is highly dynamic among MreB family proteins

We evaluated the assembled structures of PrS-SpeMreB1 after the polymerization of its monomeric fraction by adding ATP. PrS-SpeMreB1 formed sheet and bundle structures in the presence of ATP (Fig. 1C), whereas only sheets were formed at lower protein or higher salt concentrations (Fig. 1D, S1H). These results indicate that PrS-SpeMreB1 can form higher-order structures similar to that of SpeMreB5 (*25*). In contrast, PrS-SpeMreB1 did not form polymerized structures under nucleotide-free (Nf) conditions (Fig. S1I–J).

Next, to evaluate the polymerization activity of PrS-SpeMreB1, we performed sedimentation assays based on nucleotide states and estimated each critical concentration (C_C), which is the minimum concentration required for polymerization (Fig. 1E–F, Table 1). In this assay, we used a buffer containing arginine and a high-concentration salt to prevent SpeMreB aggregation (*26*). PrS-SpeMreB1 did not precipitate under Nf conditions; however, in the presence of ATP, it precipitated within the C_C range, compatible with SpeMreB5. In contrast, PrS-SpeMreB1 was less polymerized in the presence of ADP and its C_C was 9.3-fold higher than that in the presence of ATP. This fold change was larger than the C_C differences of SpeMreB5 in the presence of ATP and ADP (2.8-fold). PrS-SpeMreB1 hardly polymerized in the presence of AMPPNP (a non-hydrolyzed ATP analog). The C_C of a PrS-SpeMreB1 variant, with the Thr mutation at the active center for ATP hydrolysis (PrS-SpeMreB1 T164A), was 7.3-fold higher than that of the wild-type (WT) in the presence of ATP. These results indicate that pre-ATP hydrolysis and post-phosphate (P_i) release states are unfavorable for retaining the polymerization of PrS-SpeMreB1.

Next, to evaluate the ATPase activity of SpeMreB1, we measured P_i release. Although P_i release was not detected with PrS alone, all SpeMreBs used in this study released P_i linearly over time (Fig. 1G). The P_i release rate of PrS-SpeMreB1 was not only 5.3-fold higher than that of SpeMreB5 (*26*) (Fig. 1H, Table 2) but also 2.9- and 3.1-fold higher than that of *E. coli* MreB, which has the highest P_i release rate among the studied MreB family proteins (*31*) and animal actin (*32*), respectively. Taken together, these results suggest that the polymerization of SpeMreB1 is highly dynamic among the MreB family proteins. The P_i release rate of PrS-SpeMreB1 T164A was 200-fold lower than that of the WT, confirming that SpeMreB1 has an ATP hydrolysis mechanism common to other MreB family proteins, as previously suggested (*26*).

The linearity of the time-course P_i release measurements suggests a fetal cycle in which ATP is consumed by SpeMreB monomers, similar to *Geobacillus stearothermophilus* MreB (GsMreB) (*33*) (Fig. 1G). To confirm this, we created polymerization-deficient variants of SpeMreB1 and SpeMreB5 and measured their P_i release. Referring to the crystal structure of the SpeMreB3-AMPPNP complex, the E285 residue electrostatically interacts with the positively charged side of the α-helix starting from V216 (*26*). The corresponding residue of SpeMreB3 E285 is conserved in SMreBs, including SpeMreB1 and SpeMreB5 (E275 and E271 for SpeMreB1 and SpeMreB5, respectively) (*15*) (Fig. 1I). Therefore, we generated PrS-SpeMreB1 E275R and SpeMreB5 E271R as polymerization-deficient variants. These variants were not polymerized, even at a concentration at which polymerization was confirmed in the corresponding WTs (Fig. S1F). PrS-SpeMreB1 E275R and SpeMreB5 E271R exhibited ATPase activities that were 1.7- and 2.3-fold lower, respectively, than those of the corresponding WTs. The decrease in the P_i release rate in the polymerization-deficient variant of SpeMreB5 is consistent with the results of a previous study (*27*). These results indicate that SpeMreB1 and SpeMreB5 also possess fetal cycles similar to those of GsMreB (*33*) and that these ATPase activities are promoted by polymerization.

Polymerization of SpeMreB5 is required for the binding between SpeMreB1 and SpeMreB5

Next, we evaluated the interactions between SpeMreB1 and SpeMreB5. However, under mixed conditions of monomeric WTs, it was difficult to distinguish whether the obtained signals were derived from their interactions or promoted polymerization using any method. Therefore, we used polymerization-deficient SpeMreB1 variants to detect their interactions with SpeMreB5. In addition to the PrS-SpeMreB1 E275R variant, we analyzed the interaction of PrS-SpeMreB1 WT eluted in the void fraction at gel filtration (PSMB1v) (Fig. 1B). PSMB1v formed spherical structures of different sizes (Fig. S2B–C) and precipitated less in the sedimentation assays (Fig. S2D), regardless of the presence of ATP, suggesting that PSMB1v is a polymerization-deficient variant. Nevertheless, PSMB1v retained several characteristics of the PrS-SpeMreB1 monomer, as confirmed by the following two results: the presence of the ATPase activity, although its P_i release rate was 3.2-fold lower than that of the PrS-SpeMreB1 monomer (Table2, Fig. 1G–H); and the consistent secondary structural content, where only the α-helix content was 4.3% lower than that of the PrS-SpeMreB1 monomer, as estimated by circular dichroism (CD) measurements (Table 3, Fig. S2E). Therefore, we used PSMB1v to analyze its interaction with SpeMreB5.

Both PSMB1v and PrS-SpeMreB1 E275R were precipitated by ultracentrifugation in the presence of ATP-polymerized SpeMreB5 (Fig. 2A–B). As expected, PrS itself did not precipitate, even in the presence of SpeMreB5 and/or ATP (Fig. S3A). These results indicate that SpeMreB1 can bind to SpeMreB5 filaments, which is not caused by the aggregation of PSMB1v or the E275R mutation. The deletion of SpeMreB5 C-terminal nine residues involved in the membrane binding (SpeMreB5 ΔC9 variant) (*27*) did not affect the precipitate amount of PSMB1v (Fig. 2A second top gel, 2B), indicating that the C-terminal region of SpeMreB5 did not affect the affinity between SpeMreB1 and SpeMreB5 filaments.

Next, we attempted to detect the interaction between SpeMreB5 monomers and SpeMreB1. Due to the large size of PSMB1v, the precipitation of PSMB1v became obvious at a high concentration. Using this property, we performed co-sedimentation assays of PSMB1v and monomeric SpeMreB5 WT under Nf conditions or SpeMreB5 E271R over the nucleotide states (Fig. 2C). However, most SpeMreB5 molecules remained in the supernatant under all conditions. In addition, we performed co-sedimentation assays with PrS-SpeMreB1 WT and SpeMreB5 E271R in the presence of ATP to study the interaction between polymerized SpeMreB1 and SpeMreB5 monomers (Fig. 2D). Most SpeMreB5 E271R molecules remained in the supernatant, whereas PrS-SpeMreB1 precipitated. These results indicate that SpeMreB5 monomers do not interact with PSMB1v or polymerized PrS-SpeMreB1. The interaction between the SpeMreB5 monomer and SpeMreB1 variants was further assessed using size-exclusion chromatography (Fig.

2E–F). The peak positions and magnitudes did not change in the mixed conditions of PSMB1v or PrS-SpeMreB1 and SpeMreB5 compared with when each was independently loaded. Together, these results indicate that the polymerization of SpeMreB5 is required for the interaction between SpeMreB1 and SpeMreB5.

In addition to SpeMreB1, we performed sedimentation assays of PrS-SpeMreB4 eluted in the void fraction (Fig. 1B). Although PrS-SpeMreB4 precipitated regardless of ATP (Fig. S1G), filamentous structures were not formed, even in the presence of ATP (Fig. S1K), suggesting that PrS-SpeMreB4 precipitation in the sedimentation assays was caused by PrS-SpeMreB4 aggregation rather than polymerization. Therefore, we excluded PrS-SpeMreB4 from further analyses.

SpeMreB1 decreases SpeMreB5 filament amount depending on the nucleotide states

A previous study demonstrated that SMreB1 expressed in *E. coli* cells inhibited the filament formation of SMreB2, which was co-expressed as a model of a phylogenetic group including SMreB5 (*34*). Inspired by this study, we evaluated the effects of SpeMreB1 on SpeMreB5 filaments using co-sedimentation assays in the presence of different nucleotides (Fig. 3A–B, S3B–D). In the presence of ATP, the amount of SpeMreB5 precipitate did not change when mixed with approximately thrice higher concentrations of PrS-SpeMreB1 or PSMB1v. Intriguingly, in the presence of ADP or AMPPNP, the amount of SpeMreB5 precipitate decreased in the presence of PrS-SpeMreB1 or PSMB1v. In these nucleotide states, SpeMreB5 mostly did not precipitate in the presence of twice the concentration of PrS-SpeMreB1 or PSMB1v. This phenomenon was also consistent with PrS-SpeMreB1 E275R in the presence of ADP (in the presence of AMPPNP and PrS-SpeMreB1 E275R, the precipitation of SpeMreB5 did not decrease below 55%). In contrast, the precipitate decrease in SpeMreB5 by PrS under conditions corresponding to SpeMreB1 variants remained at 26.1% and 28.1% in the presence of ADP and AMPPNP, respectively.

These results suggest that SpeMreB1 may function as a molecular motor to dissociate SpeMreB5 filaments like kinesin-13 that promote the depolymerization of microtubules (*35*). Conventional eukaryotic motor proteins accelerate the ATPase activity by interacting with their partner cytoskeleton proteins (*36*). To know if this is the case for SpeMreBs, we measured P_i release of different concentrations (2–4 μM) of PrS-SpeMreB1 and PSMB1v in the presence of 3 μM constant SpeMreB5 (Fig. 3C). The P_i release rate constants of PrS-SpeMreB1 and PSMB1v, estimated from the linear fit slopes, were not significantly different in the presence or absence of SpeMreB5 (Fig. 3D). This was the case for the P_i release rate of 3 μM SpeMreB5 estimated from the intercept differences between the linear fits of datasets in the presence or absence of an SpeMreB1 variant (Fig. 3E). These results indicate that SpeMreB1 decreases SpeMreB5 filament amount without altering the ATPase activity.

SpeMreB1 polymerization is required for *Spiroplasma* swimming

The above experiments revealed that the polymerization-deficient variant of SpeMreB1 partially retained the ATPase activity, interaction with SpeMreB5 filaments, and the ability to decrease SpeMreB5 filaments (Fig. 1G–H, 2A–B, 3A–B). To examine the significance of SpeMreB1 polymerization in *Spiroplasma* swimming, we investigated the swimming behavior of cells expressing an SpeMreB1 variant with SpeMreB5 WT using the reconstitution system of the minimal synthetic bacterium JCVI-syn3B (*14*).

Although Syn3B cells co-expressing SpeMreB1 WT and SpeMreB5 WT were motile, similar to *Spiroplasma*, those co-expressing SpeMreB1 E275R and SpeMreB5 WT were not (Fig. 4A–B). Protein profile analysis revealed that bands corresponding to the SpeMreB1 variant and SpeMreB5 WT were detected in both strains (Fig. 4C, Table S1), suggesting that the loss of swimming motility in the strain co-expressing SpeMreB1 E275R and SpeMreB5 WT was not

caused by an aberrant SpeMreB expression. These results indicate that SpeMreB1 polymerization is essential for *Spiroplasma* swimming.

SpeMreB1 binds to negatively charged lipids in any nucleotide states

As the motility machinery of *Spiroplasma* is present underneath the cell membrane (*13, 37-39*), it is important to study the membrane-binding ability of each component of the motility machinery to understand the molecular mechanism of *Spiroplasma* swimming. Although the membrane binding of SMreB1 is largely unclear, its binding to negatively charged lipids has been experimentally demonstrated for SMreB5 (*27*). Therefore, we investigated the membrane binding of PrS-SpeMreB1. The experiments were conducted by co-sedimentation assays of SpeMreB and liposomes without arginine and a high-concentration salt for the ease of liposome handling. In addition, we decreased the centrifugal speed in the sedimentation assays without liposomes (from 436,000 ×*g* to 100,000 ×*g*) to reduce the background precipitates of SpeMreB aggregates and filaments. PrS-SpeMreB1 and PSMB1v co-precipitated with liposomes with a lipid composition mimicking that of the *Spiroplasma* cell membrane (SpiroLipid liposome), whereas PrS did not (Fig. 5A). This result indicates that SpeMreB1 binds to the membrane, contrary to our previous prediction based on the absence of membrane-binding sequences common to MreB family proteins in almost SMreB1s (*15*). The precipitated fractions of PrS-SpeMreB1, PSMB1v, and SpeMreB5 were 34.9%, 40.2%, and 51.4%, respectively (Fig. 5B), at the saturated liposome concentration, indicating that the membrane binding ability of SpeMreB1 is slightly weaker than that of SpeMreB5.

To identify the lipid molecules involved in the binding to SpeMreB1, we performed liposome binding assays of PrS-SpeMreB1 and liposomes composed of one of the following four lipids in the SpiroLipid liposome: (1,2-dioleoyl-sn-glycero-3-phospho-(1'-rac-glycerol) [DOPG], 1,2-dioleoyl-sn-glycero-3-phosphocholine [DOPC], sphingomyelin [SM], and cardiolipin [CL]) (Fig. S3F). PrS-SpeMreB1 bound to all four liposomes but strongly bound to those composed of DOPG or CL, both of which are negatively charged. To further examine the negative charge dependence of lipids for binding with SpeMreB1, we performed liposome-binding assays using PrS-SpeMreB1 and liposomes with different ratios of DOPG and DOPC. As the ratio of DOPG increased, PrS-SpeMreB1 bound strongly to the liposomes (Fig. 5C–D). These results indicate that SpeMreB1 binds to the membrane including negatively charged lipids like SMreB5 (*27*). To confirm the consistency of the negatively charged lipid dependence of the membrane binding of SpeMreB1, we modeled the structure of full-length SpeMreB1 using AlphaFold2 (*40*) (Fig. S3F). MreB is composed of four subdomains (IA, IB, IIA, and IIB) (*16, 19, 26, 27, 33, 41*), and subdomains IA and IB are involved in the membrane binding of all MreBs that have been studied previously (*20, 27*). SpeMreB1 possesses a positively charged region throughout its IA and IB subdomains, allowing it to bind to the membrane.

Next, we evaluated the membrane binding of SpeMreB1 to liposomes in the presence of nucleotides (Fig. 5E–F). Even in the presence of nucleotides, PrS-SpeMreB1 and SpeMreB5 did not precipitate at a reduced centrifugation speed in the absence of liposomes. SpeMreB5 did not bind to the liposomes in the presence of nucleotides, which is consistent with the findings of a previous study (*27*). This phenomenon was independent of polymerization, as was confirmed for SpeMreB5 E271R. In contrast, the co-precipitate amounts of PrS-SpeMreB1 and PSMB1v with liposomes were constant regardless of the nucleotide, except for PrS-SpeMreB1 in the presence of AMPPNP, in which the background precipitate increased, probably because of PrS-SpeMreB1 aggregation. These results indicate that the membrane-binding region of SpeMreB1 is still functional after binding to a nucleotide, unlike SpeMreB5.

Discussion

In this study, we solubilized SpeMreB1 by fusing it with PrS and evaluated its activity, crosstalk with SpeMreB5, and membrane binding. The β-strand content of PrS-SpeMreB1 used in this study was 8.4% higher than that predicted from its amino acid sequence (Table 3). Considering that the β-strand content of PrS, which occupies 39.1% of the residues in PrS-SpeMreB1, estimated from CD measurements was 14.1% higher than that predicted from the sequence, 5.5% of the 8.4% difference could be explained (14.1% × 0.391 = 5.5%). Excluding the effect of the high β-strand content of PrS discussed above, PrS-SpeMreB1 probably adopted the structure as predicted because the differences in α-helix and β-strand content of PrS-SpeMreB1 in experiments and prediction remained at 6.3% and 2.9%, respectively. The α-helix content differences between PrS-SpeMreB1 and PSMB1v (4.3% lower in PSMB1v than in PrS-SpeMreB1) may reflect partial denaturation of PSMB1v (Table 3). However, this structural difference had little effect on the characteristics of SpeMreB1 as PSMB1v retained the characteristic activity of PrS-SpeMreB1 (Figs. 1, 3, and 5).

Simultaneously with nucleotide-dependent polymerization (Fig. 1C–F), we found the highest fold-changes in C_C in nucleotide states and P_i release rates of PrS-SpeMreB1 in the MreB family proteins (*26*, *27*, *31-33*, *42-46*) (Tables 1 and 2). This suggests that SpeMreB1 is exceptionally dynamic in the MreB family proteins. A previous study demonstrated that SMreB1 filaments formed in *E. coli* cells were static (*34*). Our finding of SMreB1 bundles (Fig. 1C) suggests that the filaments observed in *E. coli* cells were in the form of bundles. Based on experiments using polymerization-deficient variants (Fig. 1G–I), we confirmed the existence of the ATPase fetal cycle in PrS-SpeMreB1 and SpeMreB5, as monitored in GsMreB (*33*). Time-course P_i release measurements of PrS-SpeMreB1 E275R and SpeMreB5 E271R revealed that the P_i concentration increased proportionally with time (Fig. 1G). Based on these findings, we propose an updated SpeMreB polymerization cycle (Fig. 6A). First, SpeMreBs undergo an ATPase reaction cycle in their monomeric state. During this process, P_i release is likely the rate-limiting step. During this cycle, monomeric SpeMreBs in ATP or ADP-P_i bound states initiate polymerization, leading to accelerated P_i release. In the case of SpeMreB1, most monomers probably polymerize in the ADP-P_i state, considering their low polymerization ability in the presence of AMPPNP (Fig. 1E). In contrast, SpeMreB5 displayed only two-fold differences in C_C in the presence of AMPPNP and ATP (*26*) (Table 1) and slow P_i release in the polymerization-deficient variant (Table 2, Fig. 1H), suggesting that SpeMreB5 can polymerize before hydrolyzing ATP. In this situation, SpeMreB5 follows a polymerization cycle without considering the ATPase cycle in the monomeric state, as previously described (*26*).

Polymerization of SpeMreB5 is essential for the interaction between SpeMreB1 and SpeMreB5 (Fig. 2, 6B). In addition, we found a decrease in SpeMreB5 filaments in the presence of SpeMreB1, depending on the nucleotide state (Fig. 3A–B). This result is consistent with a previous study, in which the filament formation of SMreB2, the most similar SMreB to SMreB5, in *E. coli* cells was inhibited by the co-expression of SMreB1 (*34*). PSMB1v did not interact with SpeMreB5 monomers in any nucleotide state (Fig. 3B), suggesting that SpeMreB1 does not inhibit SpeMreB5 polymerization by sequestering monomers. Assuming that MreB5 filament destabilization is involved in the force generation cycle of *Spiroplasma* swimming, it is plausible that SpeMreB1 destabilizes SpeMreB5 filaments, rather than inhibiting polymerization, which stalls the polymerization dynamics. Polymerization of SpeMreB1 was essential for *Spiroplasma* swimming (Fig. 4), suggesting that the interaction between polymerized SpeMreB1 and SpeMreB5 is involved in force generation for this motility. Although the decrease in SpeMreB5 filaments by SpeMreB1 depended on their nucleotide states, the atomic structures of SMreB5 were not substantially different between the ADP- and AMPPNP-bound states (*27*). Therefore, differences in the mechanical properties of SpeMreB5 filaments across nucleotide states, rather than structures specific to nucleotide states, may be the cause of the decrease in filament amount by SpeMreB1. A previous study has reported that actin filaments become flexible upon P_i release,

whereas their structure remains largely unchanged. The change in the mechanical properties of actin filaments is believed to affect the specificity of actin-binding proteins, such as cofilin, which selectively severs actin filaments in the ADP-bound state (*47*).

We found that SpeMreB1 bound to a membrane containing negatively charged lipids (Fig. 5). In walled bacteria, MreB is known to bind to the membrane via an amphipathic helix at the N-terminus and/or consecutive hydrophobic residues in the hydrophobic loop region (*20*). Because most SMreB1s and SMreB4s do not possess these sequences, we predicted that SMreB1 and SMreB4 would not bind to the membrane (*15*). However, SpeMreB1 bound to the membrane even without the membrane-binding regions common to walled-bacterial MreB (Fig. 5). This finding suggests that the polymerization dynamics and the activity corresponding to the decrease in the number of SpeMreB5 filaments occur underneath the cell membrane. In addition, SMreB5 binds to the membrane via its positively charged C-terminal region, which has not been reported in the MreBs of walled bacteria (*27*). These findings suggest that SMreB1 and SMreB5 have evolved unique membrane-binding abilities for driving *Spiroplasma* swimming. In this study, we confirmed the dissociation of SMreB5 from the membrane in the presence of a nucleotide (Fig. 5E–F), although independently expressed SMreB1 and SMreB5 in *Mycoplasma mycoides* localized underneath the cell membrane as filaments (*13*). This inconsistency suggests that other factors that are not reproducible in *in vitro* liposome-binding assays, such as membrane curvature and the excluded volume effect, may control the membrane binding of SMreB filaments.

In conclusion, we demonstrated the dynamic properties, membrane-binding ability, and crosstalk with SpeMreB5 filaments of SpeMreB1. These findings suggest that SpeMreB1 functions as a “molecular motor” to exert the force on a “cytoskeleton” composed of relatively static SpeMreB5 filaments to propel *Spiroplasma* swimming.

Materials and Methods

Phylogenetic analysis. The phylogenetic tree (Fig. S1B) was constructed using the maximum likelihood method based on all SMreB1 and SMreB4 sequences reported on March 3, 2021, as previously described (*15*). Bootstrap supports were estimated from 1,000 alignment samples. Ancestor estimation was performed using MEGA-X, as described previously (*15, 48*).

Cloning and expression of SpeMreB. Constructs for the expression of SpeMreB1, SpeMreB4, and SpeMreB5 fused with a 6× His-tag were prepared as the fusions of these genes with codon optimization for *E. coli* expression and a pCold-15b vector, as described in our previous study (*26*). Expression plasmids for SMreB1 and SMreB4 were constructed as fusions of pCold-15b as described previously (*26*). The plasmid for co-expressing SpeMreB4 and SpeMreB5 was constructed by inserting the codon-optimized *spemreB5* gene with the 5’-extension of GGATCCTAATTTTGTTTAACTTTAAGAAGGAGATAT, which carries an *E. coli* ribosome-binding site to the downstream of the codon-optimized *spemreB4* gene in pCold-15b. To construct expression plasmids for PrS-SpeMreB1 and PrS-SpeMreB4, the codon-optimized genes for *E. coli* expression were excised using NdeI and BamHI restriction enzymes and inserted into pCold-PrS (provided by Dr. Yoshihiro Yamaguchi, Osaka Metropolitan University, Japan), in which two consecutive PrS molecules are fused to the N-terminus of the protein of interest (Supplementary Data 1) and expressed by the pCold expression system with the selective marker of ampicillin. These SpeMreBs carry the N-terminal extension MNHKVHHHHHHMANITVFYNEDFQGKQVDLPPGNYTRAQLAALGIENNTISSVKVPPGVKAILYQNDGFAGDQIEVVANAEELGPLNNNVSSIRVISVPVQPRMANITVFYNEDFQGKQVDLPPGNYTRAQLAALGIENNTISSVKVPPGVKAILYQNDGFAGDQIEVVANAEELGPLNNNVSSIRVISVPVQPRGTIEGRH and the C-terminal extension GSRGEIHHHHHH. An empty pCold-PrS vector was used to express PrS. Each construct was transformed into *E. coli* BL21 (DE3) cells. The *E. coli* strains were grown overnight in the Luria–Bertani (LB) medium in

the presence of 50 μg/mL ampicillin at 37°C. The overnight culture was diluted with fresh LB medium containing 50 μg/mL ampicillin and incubated at 37°C. Protein expression was induced at the growth point with an OD_{600} of 0.4–0.6 in the presence of 1 mM IPTG for 24 h at 15°C. Cells were harvested, washed twice with phosphate-buffered saline (PBS) (10 mM Na_2HPO_4, 2 mM NaH_2PO_4, 3 mM KCl, and 137 mM NaCl), and stored at □80°C until needed.

Purification of SpeMreB. SpeMreB1, SpeMreB4, SpeMreB5, and their variants were purified by Ni^{2+}-NTA affinity chromatography and gel filtration as previously described (*26, 49*), independent of fusion with PrS. Briefly, cell pellets were resuspended in His trap buffer A (50 mM Tris-HCl pH 8.0, 300 mM NaCl, 50 mM imidazole-HCl pH 8.0), centrifuged at 12,000 ×*g* for 30 min at 4°C, and purified using HisTrap HP 5 mL (Cytiva; Wauwatosa, WI, USA). The imidazole concentration in the elution buffer for SpeMreB1 was changed from that used for SpeMreB5 (230 mM) to 500 mM because of the presence of double 6×His tags. The purified SpeMreBs were further subjected to HiLoad 26/600 Superdex 200 pg (Cytiva) in the gel filtration buffer (20 mM Tris-HCl pH 8.0, 300 mM NaCl) at 4°C. PrS was purified by Ni^{2+}-NTA affinity chromatography using the same procedure as that used for SpeMreBs. Protein concentrations were determined from the absorbance at 280 nm measured using a NanoDrop One (Thermo Fisher Scientific), with the absorption coefficients estimated from ProtParam, as previously described (*49*).

Electron microscopy. A 4 μL sample drop was placed onto a 400-mesh copper grid coated with carbon for 1 min at room temperature (23–27°C), washed with 10 μL water, stained with 2% (w/v) uranyl acetate for 45 s, air dried, and observed under a JEOL JEM-1010 transmission electron microscope (Tokyo, Japan) at 80 kV equipped with a FastScan-F214T charge-coupled device camera (TVIPS; Gauting, Germany).

Sedimentation assays. Samples were prepared in the previously described buffer S (20 mM Tris-HCl pH 8.0, 1 M NaCl, 200 mM L-arginine-HCl pH 8.0, 5 mM DTT, 2 mM $MgCl_2$ and 2 mM of the desired nucleotide), which prevented aggregation and polymerization in the absence of nucleotides, as confirmed by SpeMreB3 and SpeMreB5 (*26*). Co-sedimentation assays containing two of SpeMreB1, SpeMreB5, and PrS in the same sample solution were performed using this method. Sample incubation was initiated by mixing the sample solution with the desired protein concentration in gel filtration buffer and a reaction premix containing the other reagents in buffer S. After incubation at room temperature for 3 h, which was long enough to reach the equilibrium state of the polymerizations as confirmed by SpeMreB3 and SpeMreB5 (*26*), the samples were subjected to ultracentrifugation at 100,000 rpm at 23°C using a TLA-100 rotor (Beckman Coulter). The centrifugation time was set to 90 min (for samples containing PrS-SpeMreB1 variants) or 120 min (for samples without PrS-SpeMreB1), which is short enough to minimize the precipitation of SpeMreB monomers unless otherwise stated. After removal of the supernatant, the pellet was resuspended in 200 μL of water. The supernatant and pellet fractions were analyzed by SDS-PAGE on a 12.5% Laemmli gel and stained with Coomassie Brilliant Blue R-250. Of note, when preparing PrS-SpeMreB1-containing samples for SDS-PAGE, we omitted the steps of heat shock (at 95°C for 3 min in our laboratory protocol) or overnight incubation (at room temperature for more than 7 h in our laboratory protocol) after mixing with an SDS-PAGE sample solution (5% [v/v] glycerol, 0.025% [w/v] bromophenol blue, 62.5 mM Tris-HCl pH 6.8, 2.5% [w/v] sodium dodecyl sulfate, 5% [v/v] β-mercaptoethanol in our laboratory recipe), which are widely used for protein denaturation (*50*), because we have the following two experiences; (I) these steps stimulate the aggregation of PrS-SpeMreB1 in the SDS-PAGE sample solution and smearing of PrS-SpeMreB1 bands (Fig. S2F); and (II) all proteins used in this study were denatured immediately after mixing with the SDS-PAGE sample solution, as confirmed by the

small amounts of smeared bands (see gel images in this paper, except Fig. S2F, in which the SDS-PAGE samples were prepared by the 95°C heat shock). The concentrations of the supernatant and pellet fractions were estimated as the product of the total SpeMreB concentration, and the ratio of each fraction to the sum of the supernatant and pellet fractions was measured using the ImageJ software (National Institutes of Health; http://rsb.info.nih.gov/ij/). The critical concentration was estimated as the x-intercept of the linear fit with the amount of precipitate at steady-state polymerization versus the total SpeMreB concentration.

P_i release assays. P_i release measurements were performed as previously described in a standard buffer for SpeMreB polymerization (20 mM Tris-HCl pH 7.5, 100 mM KCl, 5 mM DTT, 2 mM $MgCl_2$, and 2 mM ATP) (*26*, *49*). Briefly, P_i release was detected using 2-amino-6-mercapto-7-methylpurine riboside, a molecular probe for P_i that reacts with P_i to produce a molecule that absorbs light at 360 nm.

Circular dichroism (CD). CD was measured for a 200 μL sample in a 1 mm thick quartz cuvette by J720W (JASCO; Tokyo, Japan) with a wavelength range of 200–250 nm under a nitrogen gas flow of 6 L/min at 20°C maintained by a temperature stabilizer. The measured CD intensities were converted to the mean residue ellipticities (*MRE*) using the following equation:

$$MRE\ (deg\ \ cm^2\ dmol^{-1}) = \frac{CD\ (mdeg)}{N \cdot C\ (M) \cdot l\ (mm)} \cdots (1),$$

where *N* is the number of amino acid residues in the protein of interest, *C* is the protein concentration (*M*), and *l* is the path length of the cuvette used for measurements (mm). Secondary structure contents were estimated using BeStSeL (*51*-*53*) and compared with those estimated from the amino acid sequences using PSIPRED4 (*54*).

Size-exclusion chromatography to study the interactions between SpeMreB1 and SpeMreB5. The samples were mixed in the gel filtration buffer to obtain the desired protein concentrations and incubated on ice for 1 h. A 100 μL sample solution was loaded onto Superdex™ 200 Increase 3.2/300 (Cytiva) equilibrated by the gel filtration buffer at 4°C. Protein signals were detected by measuring the absorbance at 280 nm.

Protein expression in JCVI-syn3B. The construct for transferring *spemreB1* and *spemreB5* into the genome of *Mycoplasma mycoides* JCVI-syn3B (GenBank: CP069345.1) was assembled using pSD079 (*55*) and three DNA fragments: 496,781–498,064, including *spemreB1* and its promoter*;* 1,353,199–1,353,517, including the promoter of *spemreB4*; and 1,354,572–1,355,801, including *spemreB5* and its terminator. These fragments were amplified from the *S. eriocheiris* genome (GenBank: GCA_002028345.1) (*56*). Constructs for *spemreB1* E275R and *spemreB5* were prepared by inducing a mutation in pSD079 carrying *spemreB1* WT and *spemreB5* WT. pSD128 was used as a control strain carrying the puromycin resistance gene *puroR*. Each construct was transferred into JCVI-syn3B (*57*) (*58*) as previously described (*14*). These strains were cultured in the SP4 medium at 37°C to 0.03–0.04 at OD_{620}. For protein profiling, the cell suspensions were concentrated 20-fold after washing with PBS containing sucrose (PBS/S) (75 mM sodium phosphate [pH 7.3], 68 mM NaCl, and 20 mM sucrose) and analyzed by SDS-PAGE. Protein bands were identified as previously described (*37*).

Optical microscopy and video analyses of JCVI-syn3B cells. The cultures were centrifuged at 9000 ×*g* for 8 min at 10°C. The cell pellets were resuspended in PBS/S at one-fifth the volume of

the culture, mixed with methylcellulose in PBS/S to a final concentration of 0.2%, and inserted into the tunnel slides. After 5 min at 25°C, 0.4% methylcellulose in PBS/S was inserted into the tunnel slide to wash out floating cells, and cells remaining near the glass surface were observed using an inverted microscope IX71 (Olympus; Tokyo, Japan) equipped with a UPlanSApo 100 × 1.4 numerical aperture (NA) Ph3 and complementary metal-oxide-semiconductor (CMOS) camera, DMK33UX174 (The Imaging Source Asia Co., Ltd. Taipei, Taiwan). The video was analyzed using the empirical gradient threshold (EGT) plugin (*59*) and a color footprinting macro (*60*) of ImageJ ver.1.53f51 (Fiji) (*61*).

Liposome preparation. Chloroform solutions of 10 mg/mL DOPG (840475C, Avanti Polar Lipid, Alabaster, AL, USA), DOPC (850375C, Avanti Polar Lipid), SM (860062C, Avanti Polar Lipid), and CL (710335C, Avanti Polar Lipid) were used for liposome construction. For SpiroLipid liposomes, chloroform solutions of these lipids were mixed in a previously described molar ratio (*16*, *62*) (DOPG:DOPC:SM:CL = 0.38:0.14:0.33:0.15). For liposome preparation, a chloroform solution with the desired lipid composition was aliquoted into a clean glass bottle and was completely dried by N_2 gas flow and a vacuum desiccation at room temperature. The remaining lipid layer was hydrated at room temperature using a standard buffer with increasing KCl concentration to 200 mM (to reduce the background precipitation of SpeMreBs) containing 1 mM $MgCl_2$ (for efficient liposome construction) and subjected to water bath sonication for 1 min. The liposome solution was extruded at room temperature using a 100 nm polycarbonate membrane (610005, Avanti Polar Lipid). The liposome solution was stored at 4°C and used within 2 days of the construction.

Liposome binding assays. SpeMreB samples were dialyzed to 20 mM Tris-HCl pH 7.5, 200 mM KCl, 1 mM $MgCl_2$ at 4°C for overnight. The dialyzed samples were centrifuged at 20,000 ×*g* for 10 min at 4°C to remove aggregates, mixed with a liposome solution with a final SpeMreB concentration of 2 μM and a final sample volume of 200 μL, and incubated for 15 min at room temperature. For liposome binding assays in the presence of a nucleotide, SpeMreBs were incubated in the presence of a nucleotide for 5 min at room temperature before liposome addition at twice the SpeMreB and nucleotide concentrations (4 μM and 2 mM, respectively). The incubated samples were centrifuged at 48,000 rpm (approximately 100,000 ×*g*) for 30 min at 23°C using a TLA-100 rotor. The supernatant was removed, and the pellet was resuspended in water. SpeMreB concentrations in each fraction were estimated by SDS-PAGE and subsequent image analysis as described in “Sedimentation assays” in the Materials and Methods section.

References

1. M. Miyata, R. C. Robinson, T. Q. P. Uyeda, Y. Fukumori, S. Fukushima, S. Haruta, M. Homma, K. Inaba, M. Ito, C. Kaito, K. Kato, T. Kenri, Y. Kinosita, S. Kojima, T. Minamino, H. Mori, S. Nakamura, D. Nakane, K. Nakayama, M. Nishiyama, S. Shibata, K. Shimabukuro, M. Tamakoshi, A. Taoka, Y. Tashiro, I. Tulum, H. Wada, K. Wakabayashi, Tree of motility - A proposed history of motility systems in the tree of life. *Genes to Cells* **25**, 6-21 (2020).
2. N. Wadhwa, H. C. Berg, Bacterial motility: machinery and mechanisms. *Nature reviews Microbiology* **20**, 161-173 (2022).
3. J. Royet, D. Gupta, R. Dziarski, Peptidoglycan recognition proteins: modulators of the microbiome and inflammation. *Nature reviews. Immunology* **11**, 837-851 (2011).
4. J. Royet, R. Dziarski, Peptidoglycan recognition proteins: pleiotropic sensors and effectors of antimicrobial defences. *Nature reviews Microbiology* **5**, 264-277 (2007).
5. Y. Kawai, K. Mickiewicz, J. Errington, Lysozyme counteracts β-Lactam antibiotics by promoting the emergence of L-form bacteria. *Cell* **172**, 1038-1049.e1010 (2018).

6. J. Ou, H. Dong, X. Luan, X. Wang, Q. Liu, H. Chen, M. Cao, Z. Xu, Y. Liu, W. Zhao, iTRAQ-based differential proteomic analysis of high- and low-virulence strains of Spiroplasma eriocheiris. *Microbial pathogenesis* **184**, 106365 (2023).
7. W. Wang, L. Rong, W. Gu, K. Du, J. Chen, Study on experimental infections of Spiroplasma from the Chinese mitten crab in crayfish, mice and embryonated chickens. *Research in microbiology* **154**, 677-680 (2003).
8. M. J. Daniels, P. G. Markham, B. M. Meddins, A. K. Plaskitt, R. Townsend, M. Bar-Joseph, Axenic culture of a plant pathogenic *Spiroplasma*. *Nature* **244**, 523-524 (1973).
9. R. M. Cole, J. G. Tully, T. J. Popkin, J. M. Bové, Morphology, ultrastructure, and bacteriophage infection of the helical mycoplasma-like organism (*Spiroplasma citri* gen. nov., sp. nov.) cultured from "stubborn" disease of citrus. *Journal of bacteriology* **115**, 367-384 (1973).
10. P. M. Ryan, J. W. Shaevitz, C. W. Wolgemuth, Bend or twist? What plectonemes reveal about the mysterious motility of *Spiroplasma*. *Physical review letters* **131**, 178401 (2023).
11. H. Wada, R. R. Netz, Hydrodynamics of helical-shaped bacterial motility. *Physical review E* **80**, 021921 (2009).
12. J. W. Shaevitz, J. Y. Lee, D. A. Fletcher, *Spiroplasma* swim by a processive change in body helicity. *Cell* **122**, 941-945 (2005).
13. C. Lartigue, B. Lambert, F. Rideau, Y. Dahan, M. Decossas, M. Hillion, J.-P. Douliez, J. Hardouin, O. Lambert, A. Blanchard, L. Béven, Cytoskeletal components can turn wall-less spherical bacteria into kinking helices. *Nat Commun* **13**, 6930 (2022).
14. H. Kiyama, S. Kakizawa, Y. Sasajima, Y. O. Tahara, M. Miyata, Reconstitution of a minimal motility system based on *Spiroplasma* swimming by expressing two bacterial actins in synthetic minimal bacterium. *Science advances* **8**, eabo7490 (2022).
15. D. Takahashi, I. Fujiwara, M. Miyata, Phylogenetic origin and sequence features of MreB from the wall-less swimming bacteria *Spiroplasma*. *Biochemical and biophysical research communications* **533**, 638-644 (2020).
16. S. Harne, S. Duret, V. Pande, M. Bapat, L. Béven, P. Gayathri, MreB5 is a determinant of rod-to-helical transition in the cell-wall-less bacterium *Spiroplasma*. *Current biology : CB* **30**, 4753-4762.e4757 (2020).
17. C. Ku, W. S. Lo, C. H. Kuo, Molecular evolution of the actin-like MreB protein gene family in wall-less bacteria. *Biochemical and biophysical research communications* **446**, 927-932 (2014).
18. H. Shi, B. P. Bratton, Z. Gitai, K. C. Huang, How to build a bacterial cell: MreB as the foreman of *E. coli* construction. *Cell* **172**, 1294-1305 (2018).
19. F. van den Ent, T. Izore, T. A. Bharat, C. M. Johnson, J. Löwe, Bacterial actin MreB forms antiparallel double filaments. *eLife* **3**, e02634 (2014).
20. J. Salje, F. van den Ent, P. de Boer, J. Löwe, Direct membrane binding by bacterial actin MreB. *Mol Cell* **43**, 478-487 (2011).
21. S. Middlemiss, M. Blandenet, D. M. Roberts, A. McMahon, J. Grimshaw, J. M. Edwards, Z. Sun, K. D. Whitley, T. Blu, H. Strahl, S. Holden, Molecular motor tug-of-war regulates elongasome cell wall synthesis dynamics in *Bacillus subtilis*. *Nat Commun* **15**, 5411 (2024).
22. S. van Teeffelen, S. Wang, L. Furchtgott, K. C. Huang, N. S. Wingreen, J. W. Shaevitz, Z. Gitai, The bacterial actin MreB rotates, and rotation depends on cell-wall assembly. *Proceedings of the National Academy of Sciences of the United States of America* **108**, 15822-15827 (2011).
23. J. M. Wagstaff, V. J. Planelles-Herrero, G. Sharov, A. Alnami, F. Kozielski, E. Derivery, J. Löwe, Diverse cytomotive actins and tubulins share a polymerization switch mechanism conferring robust dynamics. *Science advances* **9**, eadf3021 (2023).

24. S. Harne, P. Gayathri, L. Béven, Exploring *Spiroplasma* biology: Opportunities and challenges. *Frontiers in Microbiology* **11**, 589279 (2020).
25. D. Takahashi, M. Miyata, I. Fujiwara, Assembly properties of bacterial actin MreB involved in *Spiroplasma* swimming motility. *Journal of biological chemistry* **299**, 104793 (2023).
26. D. Takahashi, I. Fujiwara, Y. Sasajima, A. Narita, K. Imada, M. Miyata, ATP-dependent polymerization dynamics of bacterial actin proteins involved in *Spiroplasma* swimming. *Open Biol* **12**, 220083 (2022).
27. V. Pande, N. Mitra, S. R. Bagde, R. Srinivasan, P. Gayathri, Filament organization of the bacterial actin MreB is dependent on the nucleotide state. *The Journal of cell biology* **221**, e202106092 (2022).
28. H. Kobayashi, T. Yoshida, M. Inouye, Significant enhanced expression and solubility of human proteins in *Escherichia coli* by fusion with protein S from *Myxococcus xanthus*. *Applied and environmental microbiology* **75**, 5356-5362 (2009).
29. D. Takahashi, M. Miyata, Sequence analyses of a lipoprotein conserved with bacterial actins responsible for swimming motility of wall-less helical *Spiroplasma*. *microPublication biology* **2023**, (2023).
30. W. Kaplan, P. Hüsler, H. Klump, J. Erhardt, N. Sluis-Cremer, H. Dirr, Conformational stability of pGEX-expressed *Schistosoma japonicum* glutathione S-transferase: a detoxification enzyme and fusion-protein affinity tag. *Protein science : a publication of the Protein Society* **6**, 399-406 (1997).
31. P. Nurse, K. J. Marians, Purification and characterization of *Escherichia coli* MreB protein. *Journal of biological chemistry* **288**, 3469-3475 (2013).
32. R. Melki, S. Fievez, M.-F. Carlier, Continuous monitoring of P_i release following nucleotide hydrolysis in actin or tubulin assembly uing 2-amino-6-mercapto-7-methylpurine ribonucleoside and purine-nucleoside phosphorylase as an enzyme-linked assay. *Biochemistry* **35**, 12038-12045 (1996).
33. W. Mao, L. D. Renner, C. Cornilleau, I. Li de la Sierra-Gallay, S. Afensiss, S. Benlamara, Y. Ah-Seng, H. Van Tilbeurgh, S. Nessler, A. Bertin, A. Chastanet, R. Carballido-Lopez, On the role of nucleotides and lipids in the polymerization of the actin homolog MreB from a Gram-positive bacterium. *eLife* **12**, e84505 (2023).
34. F. Masson, X. Pierrat, B. Lemaitre, A. Persat, The wall-less bacterium *Spiroplasma poulsonii* builds a polymeric cytoskeleton composed of interacting MreB isoforms. *iScience* **24**, 103458 (2021).
35. P. Risteski, M. Jagrić, N. Pavin, I. M. Tolić, Biomechanics of chromosome alignment at the spindle midplane. *Current biology : CB* **31**, R574-R585 (2021).
36. E. M. De La Cruz, E. M. Ostap, Kinetic and equilibrium analysis of the myosin ATPase. *Methods in enzymology* **455**, 157-192 (2009).
37. P. Liu, H. Zheng, Q. Meng, N. Terahara, W. Gu, S. Wang, G. Zhao, D. Nakane, W. Wang, M. Miyata, Chemotaxis without conventional two-component system, based on cell polarity and aerobic conditions in helicity-switching swimming of *Spiroplasma eriocheiris*. *Front Microbiol* **8**, 58 (2017).
38. S. Trachtenberg, L. M. Dorward, V. V. Speransky, H. Jaffe, S. B. Andrews, R. D. Leapman, Structure of the cytoskeleton of *Spiroplasma melliferum* BC3 and its interactions with the cell membrane. *Journal of molecular biology* **378**, 778-789 (2008).
39. J. Kürner, A. S. Frangakis, W. Baumeister, Cryo-electron tomography reveals the cytoskeletal structure of *Spiroplasma melliferum*. *Science* **307**, 436-438 (2005).
40. M. Mirdita, K. Schütze, Y. Moriwaki, L. Heo, S. Ovchinnikov, M. Steinegger, ColabFold: making protein folding accessible to all. *Nature methods* **19**, 679-682 (2022).

41. F. van den Ent, L. A. Amos, J. Löwe, Prokaryotic origin of the actin cytoskeleton. *Nature* **413**, 39-44 (2001).
42. D. Popp, A. Narita, K. Maeda, T. Fujisawa, U. Ghoshdastider, M. Iwasa, Y. Maéda, R. C. Robinson, Filament structure, organization, and dynamics in MreB sheets. *Journal of biological chemistry* **285**, 15858-15865 (2010).
43. J. A. Mayer, K. J. Amann, Assembly properties of the *Bacillus subtilis* actin, MreB. *Cell Motility and Cytoskeleton* **66**, 109-118 (2009).
44. G. J. Bean, K. J. Amann, Polymerization properties of the *Thermotoga maritima* actin MreB: roles of temperature, nucleotides, and ions. *Biochemistry* **47**, 826-835 (2008).
45. O. Esue, M. Cordero, D. Wirtz, Y. Tseng, The assembly of MreB, a prokaryotic homolog of actin. *Journal of biological chemistry* **280**, 2628-2635 (2005).
46. L. Blanchoin, T. D. Pollard, Mechanism of interaction of *Acanthamoeba* actophorin (ADF/Cofilin) with actin filaments. *Journal of biological chemistry* **274**, 15538-15546 (1999).
47. M. J. Reynolds, C. Hachicho, A. G. Carl, R. Gong, G. M. Alushin, Bending forces and nucleotide state jointly regulate F-actin structure. *Nature* **611**, 380-386 (2022).
48. S. Kumar, G. Stecher, M. Li, C. Knyaz, K. Tamura, MEGA X: Molecular evolutionary genetics analysis across computing platforms. *Mol Biol Evol* **35**, 1547-1549 (2018).
49. D. Takahashi, I. Fujiwara, M. Miyata, Purification and ATPase activity measurement of *Spiroplasma* MreB. *Methods in molecular biology (Clifton, N.J.)* **2646**, 359-371 (2023).
50. U. K. Laemmli, Cleavage of structural proteins during the assembly of the head of bacteriophage T4. *Nature* **227**, 680-685 (1970).
51. A. Micsonai, É. Moussong, F. Wien, E. Boros, H. Vadászi, N. Murvai, Y. H. Lee, T. Molnár, M. Réfrégiers, Y. Goto, Á. Tantos, J. Kardos, BeStSel: webserver for secondary structure and fold prediction for protein CD spectroscopy. *Nucleic acids research* **50**, W90-w98 (2022).
52. A. Micsonai, É. Bulyáki, J. Kardos, BeStSel: from secondary structure analysis to protein fold prediction by circular dichroism spectroscopy. *Methods in molecular biology (Clifton, N.J.)* **2199**, 175-189 (2021).
53. A. Micsonai, F. Wien, É. Bulyáki, J. Kun, É. Moussong, Y. H. Lee, Y. Goto, M. Réfrégiers, J. Kardos, BeStSel: a web server for accurate protein secondary structure prediction and fold recognition from the circular dichroism spectra. *Nucleic acids research* **46**, W315-w322 (2018).
54. D. W. A. Buchan, D. T. Jones, The PSIPRED protein analysis workbench: 20 years on. *Nucleic acids research* **47**, W402-W407 (2019).
55. A. M. Mariscal, S. Kakizawa, J. Y. Hsu, K. Tanaka, L. González-González, A. Broto, E. Querol, M. Lluch-Senar, C. Piñero-Lambea, L. Sun, P. D. Weyman, K. S. Wise, C. Merryman, G. Tse, A. J. Moore, C. A. Hutchison, 3rd, H. O. Smith, M. Tomita, J. C. Venter, J. I. Glass, J. Piñol, Y. Suzuki, Tuning Gene Activity by Inducible and Targeted Regulation of Gene Expression in Minimal Bacterial Cells. *ACS synthetic biology* **7**, 1538-1552 (2018).
56. N. Terahara, I. Tulum, M. Miyata, Transformation of crustacean pathogenic bacterium Spiroplasma eriocheiris and expression of yellow fluorescent protein. *Biochemical and biophysical research communications* **487**, 488-493 (2017).
57. C. A. Hutchison, 3rd, R. Y. Chuang, V. N. Noskov, N. Assad-Garcia, T. J. Deerinck, M. H. Ellisman, J. Gill, K. Kannan, B. J. Karas, L. Ma, J. F. Pelletier, Z. Q. Qi, R. A. Richter, E. A. Strychalski, L. Sun, Y. Suzuki, B. Tsvetanova, K. S. Wise, H. O. Smith, J. I. Glass, C. Merryman, D. G. Gibson, J. C. Venter, Design and synthesis of a minimal bacterial genome. *Science* **351**, aad6253 (2016).

58. F. Nishiumi, Y. Kawai, Y. Nakura, M. Yoshimura, H. N. Wu, M. Hamaguchi, S. Kakizawa, Y. Suzuki, J. I. Glass, I. Yanagihara, Blockade of endoplasmic reticulum stress-induced cell death by *Ureaplasma parvum* vacuolating factor. *Cellular Microbiology* **23**, e13392 (2021).
59. J. Chalfoun, M. Majurski, A. Peskin, C. Breen, P. Bajcsy, M. Brady, Empirical gradient threshold technique for automated segmentation across image modalities and cell lines. *J Microsc* **260**, 86-99 (2015).
60. Y. Hiratsuka, M. Miyata, T. Q. Uyeda, Living microtransporter by uni-directional gliding of *Mycoplasma* along microtracks. *Biochemical and biophysical research communications* **331**, 318-324 (2005).
61. J. Schindelin, I. Arganda-Carreras, E. Frise, V. Kaynig, M. Longair, T. Pietzsch, S. Preibisch, C. Rueden, S. Saalfeld, B. Schmid, J. Y. Tinevez, D. J. White, V. Hartenstein, K. Eliceiri, P. Tomancak, A. Cardona, Fiji: an open-source platform for biological-image analysis. *Nature methods* **9**, 676-682 (2012).
62. P. J. Davis, A. Katznel, S. Razin, S. Rottem, *Spiroplasma* membrane lipids. *Journal of bacteriology* **161**, 118-122 (1985).

Acknowledgments
We thank Ms. Junko Shiomi, Ms. Tomomi Shimonaka, Mr. Yuhei O Tahara, Dr. Ritsuko Fujii, and Dr. Yoshihiro Yamaguchi (all of whom are affiliated with the Graduate School of Science, Osaka Metropolitan University, Japan) for their technical assistance with SpeMreB construction and expression, technical assistance with MALDI-TOF MASS spectrometry, technical assistance for negative-staining EM, providing a facility for CD measurements, and pCold-PrS.

Funding: This study was supported by the JST CREST (grant number JPMJCR19S5) to MM. DT and HK are recipients of a Research Fellowship from the Japan Society for the Promotion of Science (JP22KJ2613 and JP24KJ0169 for DT and JP22KJ2608 and JP24KJ0189 for HK).

Author contributions: Conceptualization: DT and MM. Methodology: DT, HK, and HM. Investigation: DT and HK. Visualization: DT and HK. Supervision: IF and MM. Writing the original draft: DT, MM, and IF. Writing—review and editing: DT, HK, HM, MM, and IF. Funding acquisition: DT, HK, and MM.

Competing interests: Authors declare that they have no competing interests.

Data and materials availability: Raw data are available from the corresponding author upon reasonable request.

Figures and Tables

Fig. 1. Preparation and evaluation of PrS-SpeMreB1 and PrS-SpeMreB4. (**A**) Domain architecture of PrS-fused SpeMreB1 and SpeMreB4. The N-termini of SpeMreB1 and SpeMreB4 were fused with a 6×His-tag, two consecutive PrS molecules, and a Factor Xa cleavage site. The C-termini of SpeMreB1 and SpeMreB4 were fused with a 6×His-tag. The numbers underneath the figure indicate the residue numbers of PrS-SpeMreB1. (**B**) Gel filtration profiles of PrS-SpeMreB1 WT (dark yellow) and PrS-SpeMreB4 WT (black). Peak positions of PSMB1v WT and the monomeric PrS-SpeMreB1 WT are indicated by closed triangles. Bovine γ-globulin (158 kDa), chicken ovalbumin (44 kDa), and horse myoglobin (17 kDa) were used as the protein size standards, and their elution volumes are indicated by closed diamonds with the linear fit over the log of their molecular weights. (**C–D**) Negative staining EM images of 15 μM PrS-SpeMreB1 WT in (**C**) the standard buffer (20 mM Tris-HCl pH 7.5, 100 mM KCl, 5 mM DTT, 2 mM

$MgCl_2$, 2 mM ATP) and (**D**) that with the increasing KCl concentration of 500 mM. (**E**) Sedimentation assays of PrS-SpeMreB1 WT over the nucleotide states and PrS-SpeMreB1 T164A in the presence of ATP. (**F**) Quantification of pellet amounts of PrS-SpeMreB1 WT in the presence of ATP or ADP and PrS-SpeMreB1 T164A in the presence of ATP. The resulting concentrations of the precipitated fractions were plotted against the total SpeMreB concentrations with linear fitting. Error bars indicate the SD of three independent measurements. Critical concentrations were estimated as the *x*-intercept of each linear fit and are summarized in Table 1. (**G**) Time course spectra of P_i release from PrS-SpeMreB1 WT (yellow), PSMB1v WT (orange), PrS-SpeMreB1 E275R (light green), PrS-SpeMreB1 T164A (dark gray), SpeMreB5 E271R (pink), and PrS (light gray). Protein concentrations were set at 3 μM for SpeMreBs and 5 μM for PrS. Data are presented as mean ± SD of three independent measurements. (**H**) Concentration dependence of P_i release of PrS-SpeMreB1 WT (yellow), PSMB1v WT (orange), PrS-SpeMreB1 E275R (light green), PrS-SpeMreB1 T164A (dark gray), and SpeMreB5 E271R (pink). Error bars indicate the SD of three independent measurements. P_i release rates (k_{Pi}) were estimated from the slopes of the linear fits and are summarized in Table 2. (**I**) Ribbon representation of two consecutive molecules along the *a*-axis in the crystal of the SpeMreB3-AMPPNP complex (PDB: 7E1G). The intra-protofilament interaction region is magnified using the transparent surface model colored based on the surface potential map (blue and red for positive and negative charges, respectively). Residue E285 is represented using the stick model with the corresponding residue numbers in SpeMreB1, SpeMreB3, and SpeMreB5.

Fig. 2. Interaction between SpeMreB1 and SpeMreB5. For co-sedimentation assays, protein size standards were visualized in lane M with the molecular masses of each band on the left side. The band positions of prey and bait in the gel images are indicated by P and B, respectively. The result scheme of each experiment is shown as a cartoon reflecting the assembly states (monomeric, polymerized, or oligomerized), nucleotide states (empty, T, D, and M symbols for nucleotide-free, ATP, ADP, and AMPPNP, respectively), and mutations (star for the polymerization-deficient mutation and the lack of blue line for the C-terminus deletion of SpeMreB5) of PrS-SpeMreB1 (yellow circle connected with a gray circle indicating PrS) and SpeMreB5 (red circle with the C-terminal region as a blue line). (**A**) Co-sedimentation assays of PrS-SpeMreB1 and SpeMreB5 variants in the pairs indicated in each gel image in the presence of 2 mM ATP. The concentration of SpeMreB5 variants was constant at 3 μM, whereas that of PrS-SpeMreB1 variants varied from 1 μM to 6 μM. (**B**) Quantification of pellet amounts of PrS-SpeMreB1 variants in the co-sedimentation assays with the 3 μM SpeMreB5 variant. The resulting concentrations of the precipitated fractions were plotted against the total concentrations by open circles with the matched color scale to Fig. 2A. Error bars indicate the SD of three independent measurements. (**C**) Co-sedimentation assays of PSMB1v WT and SpeMreB5 WT in the nucleotide-free condition or SpeMreB5 E271R in the presence of 2 mM ATP, ADP, or AMPPNP. The concentration of PSMB1v WT was constant at 15 μM, whereas that of SpeMreB5 variants varied from 0 μM to 15 μM. The centrifugation time was set to 30 min, which was short enough to minimize the precipitation of the high concentration of SpeMreB5 monomers. (**D**) Co-sedimentation assay of 3 μM PrS-SpeMreB1 WT and 0 μM to 10 μM SpeMreB5 E271R in the presence of 2 mM ATP. (**E–F**) Size exclusion chromatography of (**E**) PSMB1v WT and (**F**) PrS-SpeMreB1 WT with SpeMreB5. Peak positions of PSMB1v WT, PrS-SpeMreB1 WT, and SpeMreB5 WT are indicated by dashed lines. Bovine thyroglobulin (670 kDa), bovine γ-globulin (158 kDa), chicken ovalbumin (44 kDa), and horse myoglobin (17 kDa) were used for the protein size standards, and their elution volumes are plotted by closed diamonds with the linear fit over the log of their molecular weights. (**E**) Gel filtration spectra of 10 μM PSMB1v WT (light orange), 10 μM SpeMreB5 WT (red), the mixture of 10 μM PSMB1v WT and 10 μM SpeMreB5 WT (brown), and the sum of spectra from independent loads of 10 μM PSMB1v WT and 10 μM SpeMreB5

WT (gray). (**F**) Gel filtration spectra of 10 μM PrS-SpeMreB1 WT (yellow), 10 μM SpeMreB5 WT (red), the mixture of 10 μM PrS-SpeMreB1 WT and 10 μM SpeMreB5 WT (dark yellow), and the sum of spectra from independent loads of 10 μM PrS-SpeMreB1 WT and 10 μM SpeMreB5 WT (gray).

Fig. 3. Effects of SpeMreB1 on SpeMreB5. (**A**) Co-sedimentation assays of 3 μM SpeMreB5 WT and 6 μM PSMB1v WT (top) or PrS-SpeMreB1 WT (bottom) in the presence of 2 mM ATP, ADP, or AMPPNP. Protein size standards were visualized in lane M with the molecular masses of each band on the left side. The band positions of prey and bait in the gel images are indicated by P and B, respectively. The result scheme of each co-sedimentation assay of PSMB1v and SpeMreB5 is shown as a cartoon reflecting the assembly states (monomeric, polymerized, or oligomerized) and nucleotide states (empty, T, D, and M symbols for nucleotide-free, ATP, ADP, and AMPPNP, respectively) of PrS-SpeMreB1 (yellow circle connected with gray circle indicating PrS) and SpeMreB5 (red circle with the C-terminal region as a blue line). (**B**) Relative pellet amounts of SpeMreB5 WT in co-sedimentation assays with an SpeMreB1 variant and a nucleotide. The total SpeMreB5 WT concentration was constant at 3 μM, whereas that of PrS-SpeMreB1 variants varied from 0 μM to 10 μM as shown in Fig. S3B–D. The resulting concentrations of the precipitated fractions were plotted against the total concentrations of an SpeMreB1 variant. The colors of the plots indicate the proteins added versus SpeMreB5 WT (yellow-, orange-, green-, and gray-scaled colors for PrS-SpeMreB1 WT, PSMB1v WT, PrS-SpeMreB1 E275R, and PrS, respectively). The shapes of the plots indicate the added nucleotide (open circles, open diamonds, and crosses for 2 mM ATP, ADP, and AMPPNP, respectively). Error bars indicate the SD from three independent measurements. (**C**) Concentration dependence of P_i release from PrS-SpeMreB1 WT (yellow-scaled colors, 1m) and PSMB1v WT (orange-scaled colors, 1v) in the presence (dark colors) or absence (light colors) of 3 μM SpeMreB5 WT. Error bars indicate the SD from three independent measurements. (**D**) P_i release rates of PrS-SpeMreB1 WT (yellow-scaled colors) and PSMB1v WT (orange-scaled colors) in the presence (dark colors) or absence (light colors) of 3 μM SpeMreB5 WT estimated from the slopes of the linear fits in Fig. 3C. Error bars indicate the SD from three independent measurements. Symbols indicate *p*-values supported by Student's *t*-test (n.s., $p > 0.05$). (**E**) P_i release rates of 3 μM SpeMreB5 WT alone (red) and in the presence of PrS-SpeMreB1 WT (dark yellow) and PSMB1v WT (brown) estimated from the intercepts of the linear fit in Fig. 3C. Error bars indicate the SD from three independent measurements. Symbols indicate *p*-values supported by Student's *t*-test (n.s., $p > 0.05$).

Fig. 4. Behavior of syn3B cells expressing an SpeMreB1 variant and SpeMreB5 WT. (**A**) (Upper) Phase-contrast field images of (left) control syn3B cells carrying the antibiotic selection maker and those co-expressing (middle) SpeMreB1 WT and SpeMreB5 WT and (right) SpeMreB1 E275R and SpeMreB5 WT. (Lower) Trajectories of cells corresponding to each upper image for 10 s. Video frames were clipped for every 1 s, colored from red to blue in a rainbow-colored manner, and superimposed onto one image. (**B**) The motile cell ratio of the syn3B stains shown in Fig. 4A counted from the cells in three individual fields (110.8 × 62.3 μms) with SD of three individual observations (911, 545, and 563 cells sum for the control cells, cells co-expressing SpeMreB1 WT and SpeMreB5 WT, and those co-expressing SpeMreB1 E275R and SpeMreB5 WT, respectively). (**C**) Protein profiles of syn3B strains analyzed by SDS-PAGE. Protein size standards were visualized in lane M with the molecular masses of each band on the left side. The proteins bands with arrowheads and roman numbers are identified by peptide mass fingerprinting using MALDI-TOF MASS and summarized in Table S1. The band positions of SpeMreB1 and SpeMreB5 are indicated by arrowheads with 1 and 5, respectively.

Fig. 5. Liposome binding of SpeMreBs. For gel images, protein size standards were visualized in lane M with the molecular masses of each band on the left side. (**A**) Liposome binding assays of 2 μM PrS-SpeMreB1 WT (top), 2 μM PSMB1v WT (second top), 2 μM SpeMreB5 WT (second bottom), and 2 μM PrS (bottom) for concentrations of SpiroLipid liposomes. (**B**) Quantification of pellet amounts in the liposome binding assays. The resulting concentrations of the precipitated fractions were plotted over the total liposome concentrations by yellow (2 μM PrS-SpeMreB1 WT), orange (2 μM PSMB1v WT), red (2 μM SpeMreB5 WT), and gray (2 μM PrS) open circles. Error bars indicate the SD of three independent measurements. (**C**) Liposome binding assay of 2 μM PrS-SpeMreB1 WT in the presence of 1 mM liposomes with different DOPC and DOPG ratios shown at the top of each lane. DOPG is labeled in red characters as indicative of its negative charge. (**D**) Quantification of pellet amounts in the liposome binding assays of 2 μM PrS-SpeMreB1 WT in the presence of 1 mM liposomes with different DOPC and DOPG ratios plotted against the DOPG ratio. Error bars indicate the SD of three independent measurements. (**E**) Liposome binding assays of 2 μM PrS-SpeMreB1 WT (top), 2 μM PSMB1v WT (second top), 2 μM SpeMreB5 WT (second bottom), and 2 μM SpeMreB5 E271R (bottom) in the presence of 1 mM SpiroLipid liposome and 1 mM nucleotide as indicated at the top of each lane (Nf, T, D, M for nucleotide-free, with ATP, with ADP, and with AMPPNP, respectively). (**F**) Quantification of pellet amounts in the liposome binding assays in the presence of 1 mM SpiroLipid liposome and 1 mM nucleotide. Precipitate concentration differences in the presence and absence of liposomes were summarized for each construct. The patterns in the bars indicate the added nucleotides (solid, diagonal stripe, horizontal stripe, and check patterns for nucleotide-free, with ATP, with ADP, and with AMPPNP, respectively). Error bars indicate the SD of three independent measurements. Symbols indicate *p*-values supported by Student's *t*-test (* $p < 0.05$, *** $p < 1.0 \times 10^{-3}$, **** $p < 1.0 \times 10^{-4}$, and n.s. $p > 0.05$).

Fig. 6. Working models and summary of SpeMreB1 molecular features. (**A**) Working model of the polymerization dynamics of SpeMreB1. The monomeric SpeMreB1 consumes ATP as the fetal cycle with the possible rate-limiting step of P_i release. During this cycle, the monomer in the ATP and/or ADP-P_i state enters the polymerization cycle with a higher P_i release rate. (**B**) Mode of SpeMreB1 binding to SpeMreB5 filaments, but not to SpeMreB5 monomers.

Table 1. Bulk critical concentrations of SpeMreBs estimated from sedimentation assays. Values in this study are indicated as the mean ± SD of three independent measurements, except for PrS-SpeMreB1 WT in the presence of AMPPNP whose critical concentrations could not be determined by the linear fitting due to the small pellet amounts.

Table 2. P_i release rates of SpeMreBs. Values in this study are indicated as the mean ± SD of three independent measurements.

Table 3. Secondary structure contents and number of amino acid residues in PrS-SpeMreB1 and PrS. The secondary structure contents in the rows labeled CD and Theor. were estimated from the CD spectra (Fig. S2E) and amino acid sequences, respectively.

Supplementary Materials

Table S1. Results of peptide mass fingerprinting of bands shown in Fig. 4C. Roman numbers indicate protein bands shown in Fig. 4C. All proteins were detected in both peptide mass fingerprinting and MS/MS analyses. The Mascot protein score is defined by −10×log(P), where P is the probability that the observed match is a random event. The reference dataset for peptide mass finger printing was prepared by adding the amino acid sequence of SpeMreB1 E275R to the

coding sequence libraries of Synthetic bacterium JCVI-syn3B (taxonomy ID: 2806337) and *Spiroplasma eriocheiris* (taxonomy ID: 743698) in the NCBI database.

Fig. S1. Preparation and evaluation of PrS-SpeMreB1 and PrS-SpeMreB4. For gel images, protein size standards were visualized in lane M with the molecular masses next to each band. (**A**) Expression of SpeMreB1 WT (left) and SpeMreB4 WT (right) without the PrS tag. The SpeMreBs were expressed by *E. coli* BL21 (DE3) as a 6×His-tag fusion at each N-terminus using the pCold-15b expression system. Cells were sonicated in 50 mM Tris-HCl (pH 8.0), 300 mM NaCl, and centrifuged at 12,000 ×*g* for 30 min at 4°C. The whole cell lysate, supernatant, and pellet fractions were analyzed by SDS-PAGE. The band positions for SpeMreB1 WT and SpeMreB4 WT are indicated by an arrowhead. (**B**) Phylogenetic tree of SMreB1 and SMreB4. The scale bar is in units of the number of amino acid substitutions per site. Sequences used for expression experiments in this study are indicated by red triangles with their labeling. (**C**) Expression of *S. melliferum* MreB4 (SmerMreB4), *S. kunkelii* MreB4 (SkuMreB4), *S. melliferum* MreB1 (SmerMreB1), *S. apis* MreB4 (SapiMreB4), *S. litorale* MreB1 (SlitMreB1), a reconstituted ancestor of the Citri clade MreB1 and MreB4 (AnCitMreB1/4), and a reconstituted ancestor of *Spiroplasma* MreB1 and MreB4 (AnSMreB1/4). These constructs were cloned, expressed, isolated, and analyzed by SDS-PAGE using the same procedures as those in Fig. S1A. The band positions of these constructs are indicated by an arrowhead. (**D**) Co-expression of 6×His-tagged SpeMreB4 WT and untagged SpeMreB5 WT and their purification. *E. coli* cells co-expressing these SpeMreB4 and SpeMreB5 constructs were sonicated in 50 mM Tris-HCl pH 8.0, 50 mM Imidazole-HCl pH 8.0, 300 mM NaCl, centrifuged at 12,000 ×*g* for 30 min at 4°C and applied to a Ni^{2+}-NTA affinity chromatography column. The following fractions were visualized by a Coomassie-stained 12.5% Laemmli gel; fraction 1: lysate of *E. coli* co-expressing SpeMreB4 WT and SpeMreB5 WT; fractions 2 and 3: soluble (2) and insoluble (3) fractions of the whole cell lysate (1); fraction 4: flow-through fraction of Ni^{2+}-NTA affinity chromatography; other fractions: elution fractions of Ni^{2+}-NTA affinity chromatography with a gradually increasing imidazole concentration. Red and black stars indicate the bands in which SpeMreB4 and SpeMreB5 were detected, respectively, by the peptide mass fingerprinting technique using MALDI-TOF MASS spectrometry. SpeMreB5 was detected in lanes 2, 3, and 4, whereas SpeMreB4 was detected in lane 3 and not detected in lane 2, indicating that SpeMreB4 remained insoluble despite co-expression with SpeMreB5. (**E**) Purification procedure of PrS-SpeMreB1 WT. The following fractions were visualized using a Coomassie-stained 12.5% Laemmli gel; fraction 1: lysate of *E. coli* expressing PrS-SpeMreB1 WT; fractions 2 and 3: soluble (2) and insoluble (3) fractions of the whole cell lysate (1); fractions 4 and 5: flow-through (4) and elution (5) fractions of Ni^{2+}-NTA affinity chromatography; the other fractions: gel filtration elution fractions with the elution volume in Fig. 1B indicated on each lane. The band position of PrS-SpeMreB1 is indicated by an arrowhead. (**F**) Sedimentation assays of PrS-SpeMreB1 E275R (top) and SpeMreB5 E271R (bottom) in the presence of 2 mM ATP. (**G**) Sedimentation assays of 5 μM SpeMreB4 WT in the presence or absence of 2 mM ATP. (**H–K**) Negative staining EM images of (**H**) 5 μM and (**I–J**) 30 μM PrS-SpeMreB1 WT and (**K**) 5 μM SpeMreB4 WT in (**H–I** and **K**) the standard buffer (20 mM Tris-HCl pH 7.5, 100 mM KCl, 5 mM DTT) and (**J**) that with the increasing KCl concentration of 500 mM in the (**H** and **K**) presence or (**I–J**) absence of 2 mM MgATP.

Fig. S2. Evaluation of PSMB1v. For gel images, protein size standards were visualized in lane M with the molecular masses next to each band. (**A**) Gel filtration profiles of 50 μM PrS by Superdex™ 200 Increase 3.2/300 in the gel filtration buffer. Bovine thyroglobulin (670 kDa), bovine γ-globulin (158 kDa), chicken ovalbumin (44 kDa), and horse myoglobin (17 kDa) were used as the protein size standards, and their elution volumes are plotted using closed diamonds

with the linear fit over the log of their molecular weights. The estimated elution volume of the monomeric PrS (23 kDa) shown as a dashed line is in good agreement with the peak top position of the PrS elution pattern, indicating that most of PrS molecules formed monomers at this concentration. (**B–C**) Negative staining EM images of 300 nM PSMB1v in the standard buffer in the (**B**) presence and (**C**) absence of 2 mM MgATP. (**D**) Sedimentation assays of 3 μM PSMB1v WT in the presence or absence of 2 mM ATP. (**E**) CD spectra of 5 μM PrS-SpeMreB1 WT (yellow), 5 μM PSMB1v WT (orange), and 5 μM PrS (gray) in the gel filtration buffer. (**F**) An example of an SDS-PAGE profile of PrS-SpeMreB1 WT in which the samples were prepared with a heat shock step. After mixing with the SDS-PAGE sample solution, PrS-SpeMreB1 in the gel filtration buffer was heated at 95°C for 3 min before loading onto the SDS-PAGE gel, and smears of PrS-SpeMreB1 bands appeared at the region indicated by half brackets. Black stars indicate the lanes in which multiple amounts of PrS-SpeMreB1 WT were stacked on top of stacking and running gels. The band position for unaggregated PrS-SpeMreB1 WT is indicated by an arrowhead.

Fig. S3. Sedimentation assays of PrS-SpeMreB1 variants. For gel images, protein size standards were visualized in Lane M with the molecular masses beside each band. The band positions of prey and bait in gel images of co-sedimentation assays are indicated by P and B, respectively. (**A**) Co-sedimentation assays of 3 μM SpeMreB5 WT and 1 μM to 5 μM PrS in the presence or absence of 2 mM ATP. (**B**) Co-sedimentation assays of 3 μM SpeMreB5 WT and 0 μM to 10 μM PSMB1v WT (top), PrS-SpeMreB1 WT (middle), or PrS (bottom) in the presence of 2 mM ATP. Pellet amounts of SpeMreB5 were estimated and summarized in Fig. 3B. (**C–D**) Co-sedimentation assays of 3 μM SpeMreB5 WT and 0 μM to 6 μM PrS-SpeMreB1 WT (top), PSMB1v WT (second top), PrS-SpeMreB1 E275R (second bottom), or PrS (bottom) in the presence of 2 mM (**C**) ADP or (**D**) AMPPNP. Pellet amounts of SpeMreB5 were estimated and summarized in Fig. 3B. (**E**) Liposome binding assays of 2 μM PrS-SpeMreB1 WT in the presence of 1 mM liposomes composed of 100% DOPG, DOPC, SM, or CL. Negatively charged lipids (DOPG and CL) are indicated by red characters. (**F**) The surface representation of the full-length SpeMreB1 monomer modeled by AlphaFold2 (*40*). The Coulombic electrostatic potential is indicated by the color gradient from blue (+10 kcal/mol/e) to red (−10 kcal/mol/e) via white (0 kcal/mol/e). Subdomains IA, IB, IIA, and IIB are indicated at the corresponding positions of the structure. The side view of the membrane binding region on most MreBs (*20*, *27*) is shown on the right beside the front view on the left.

Movie S1. Combined real-time movies (10 s) of three syn3B strains collected from phase contrast. The strain names are shown at the top left of each panel. The scale bar indicates the bottom of the right panel.

Supplementary data 1. Nucleotide sequence of multiple cloning sites in pCold-PrS. Sequences of PrS, 6xHis-tag, factor Xa cleavage site, NdeI site, and BamHI site are shown in gray, blue, brown, purple, and red, respectively. The 5'- and 3'-ends are respectively connected with 5'- and 3'-UTR of a cold shock gene, *cspA*.

ATGAATCATAAAGTG**CATCATCATCATCATCAC**ATGGCAAATATTACCGTTTTCTA
TAACGAAGACTTCCAGGGTAAGCAGGTCGATCTGCCGCCTGGCAACTATACCCG
CGCCCAGTTGGCGGCGCTGGGCATCGAGAATAATACCATCAGCTCGGTGAAGG
TGCCGCCTGGCGTGAAGGCTATCCTGTACCAGAACGATGGTTTCGCCGGCGACC
AGATCGAAGTGGTGGCCAATGCCGAGGAGTTGGGCCCGCTGAATAATAACGTC
TCCAGCATCCGCGTCATCTCCGTGCCCGTGCAGCCGCGCATGGCAAATATTACC
GTTTTCTATAACGAAGACTTCCAGGGTAAGCAGGTCGATCTGCCGCCTGGCAAC
TATACCCGCGCCCAGTTGGCGGCGCTGGGCATCGAGAATAATACCATCAGCTCG

GTGAAGGTGCCGCCTGGCGTGAAGGCTATCCTCTACCAGAACGATGGTTTCGCC
GGCGACCAGATCGAAGTGGTGGCCAATGCCGAGGAGCTGGGTCCGCTGAATAA
TAACGTCTCCAGCATCCGCGTCATCTCCGTGCCGGTGCAGCCGAGGGGTACC**AT**
TGAAGGCCGCCATATGGTCGACCTCGAG**GGATCC**CCGTGGTGAAATC**CATCACCAT**
CACCATCACTAATCTAGATAGGTAA

Supplementary data 2. Amino acid sequences and accession IDs of SMreB1 and SMreB4 used in expression experiments (Fig. S1 B–C). Accession IDs are summarized for sequences deposited in GenBank. The amino acid sequences are summarized for the other sequences.

>SpeMreB1: WP_047791301.1
>SpeMreB4: WP_047792066.1
>SmerMreB1: WP_004028643.1
>SmerMreB4: WP_004028011.1
>SkuMreB4: WP_053390367.1
>SapiMreB4: WP_023790308.1
>SlitMreB1: WP_075058542.1
>AnCitMreB1/4
MALFNSKKPTFVSMDLGTANTLVYVSGSGIVYNEPSIVAYKIKENRIIAVGNEAYKMIGK
GNKSIRIVRPMVDGVITDIRATEAQLRYIFNKLRISKQLKNSIMLLACPSVITELEKNALKK
IAMNLGADKVFVEEEVKMAALGGGVDIYKPAGNLVVDMGGGTTDIAVLASGDIVLSKS
VKVAGNYLNDEIQKFIRSQYGLEIGIKTAEQIKIEIGSLAKYPDERKMKVYGRDVVSGLPR
EIEVTPEEIREVLKVPVSRIIDLTVQVLEETPPELAGDIFRNGITICGGGALIKGIDKYFEDTL
QLPAKIGEQPLLAVINGTKKFESDIYDILRQEHMHTKELNY

>AnSMreB1/4
MAKKKSKKPTFVSMDLGTANTLVYISGQGIVYNEPSIVAYKIKENKIIAVGEEAYKMIGK
GNKNIRIVRPMVDGVITDIRATEAQLRYIFNKLRISKTLKNSIMLLACPSVITELEKNALKK
IAMNLGADKVFVEEEVKMAALGGGVNIYAPTGNLVVDMGGGTTDIAVLASGDIVLSKSI
KVAGNYLNDEIQKFIRSQYGLEIGIKTAEQIKINIGSLAKYPDERKMKVYGRDVVSGLPRE
IEITPEEIREVLKVPVSRIIDLTVQVLEETPPELAGDIFRNGITICGGGALIKGIDKYFEDTLQ
LPTKIGEQPLLAVINGTKKFESDIYDILKEEHNHTKELNY

Table 1

Construct-nucleotide	PrS-SpeMreB1 WT-ATP	PrS-SpeMreB1 WT-ADP	PrS-SpeMreB1 WT-AMPPNP	PrS-SpeMreB1 T164A-ATP	SpeMreB5 WT-ATP	SpeMreB5 WT-ADP	SpeMreB5 WT-AMPPNP	SpeMreB5 T160A-ATP
C_C (μM)	0.41 ± 0.05	3.8 ± 0.7	>= 7	3.0 ± 0.2	0.14 ± 0.07	0.39 ± 0.09	0.29 ± 0.11	0.15 ± 0.15
Reference	This study	This study	This study	This study	Takahashi D *et al*., 2022 *Open Biol*. 12(10):220083.	Takahashi D *et al*., 2022 *Open Biol*. 12(10):220083.	Takahashi D *et al*., 2022 *Open Biol*. 12(10):220083.	Takahashi D *et al*., 2022 *Open Biol*. 12(10):220083.

Table 2

Construct	PrS-SpeMreB1 WT	PSMB1v WT	PrS-SpeMreB1 E275R	PrS-SpeMreB1 T164A
k_{Pi} (nM (P_i) / s / μM (protein))	8.0 ± 0.1	2.5 ± 0.1	4.6 ± 0.1	0.04 ± 0.02
Reference	This study	This study	This study	This study

Construct	SpeMreB5 WT	SpeMreB5 E271R	SciMreB5 WT	EcMreB	Actin
k_{Pi} (nM (P_i) / s / μM (protein))	1.5 ± 0.2	0.66 ± 0.04	2.5 ± 0.1	2.8 ± 0.2	2.6 ± 0.4
Reference	Takahashi D *et al*., 2022 *Open Biol*. 12(10):220083.	This study	Pande V *et al.* 2022. *J Cell Biol.* 221(5):e20210692.	Nurse P and Marians KJ. 2013. *J Biol Chem*. 288(5):3469-75.	Melki R *et al*. 1996. *Biochemistry*. 35(37):12038-45..

Table 3

	α-helix (%)	β-strand (%)	Amino acid residues (a.a.)
PrS-SpeMreB1 (CD)	23.2	32.7	560
PSMB1v (CD)	18.9	32.7	
PrS-SpeMreB1 (Theor.)	29.5	24.3	
PrS (CD)	8.1	45.6	219
PrS (Theor.)	8.7	31.5	

Table S1

Protein band	Protein ID	Gene name	Annotation	Mascot protein score	Mass [kDa]	Sequence coverage [%]	Species
i	QWN46562.1	*gap*	Glyceraldehyde-3-phosphate dehydrogenase	39	37.2	24	Synthetic bacterium JCVI-Syn3B
ii	QWN46586.1	*rpoA*	DNA-directed RNA polymerase subunit alpha	60	35.0	45	Synthetic bacterium JCVI-Syn3B
iii	QWN46506.1*	*ldh*	L-lactate dehydrogenase	20	34.8	26	Synthetic bacterium JCVI-Syn3B
iv	AHF58343.1	*mreB5*	Cell shape-determining protein MreB	69	38.7	28	*Spiroplasma eriocheiris*
v	AHF57598.1	*mreB1*	Cell shape-determining protein MreB	53	38.0	34	*Spiroplasma eriocheiris*
vi	AHF58343.1	*mreB5*	Cell shape-determining protein MreB	51	38.7	26	*Spiroplasma eriocheiris*
vii	AHF57598.1-2	*mreB1 E275R*	Cell shape-determining protein MreB	59	38.0	30	*Spiroplasma eriocheiris*

* Although this protein did not get the highest score in the peptide mass finger printing, it was identified in the MS/MS analysis.

Fig 1

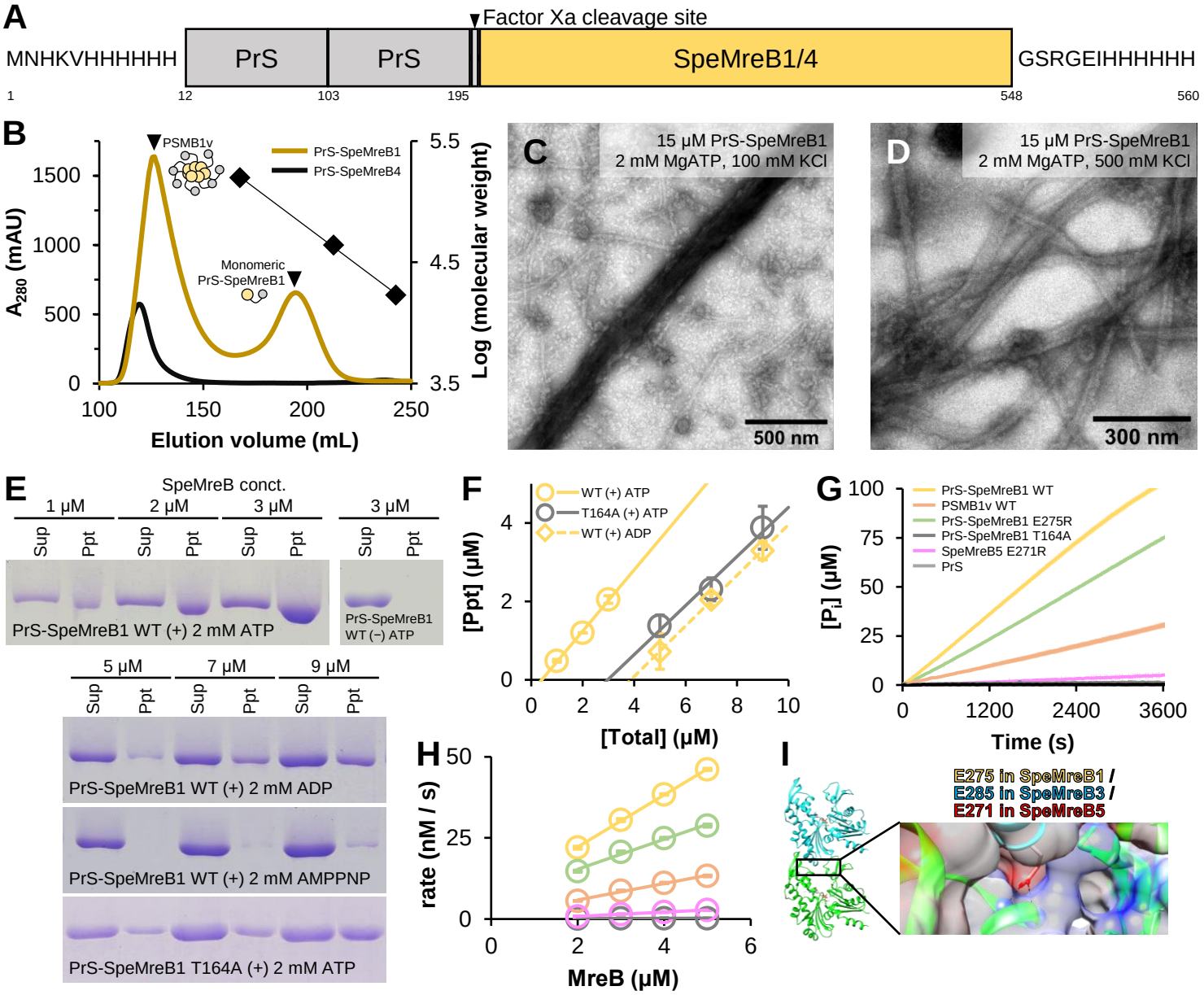
A
Factor Xa cleavage site
MNHKVHHHHHH
PrS
PrS
SpeMreB1/4
GSRGEIHHHHHH
1
12
103
195
548
560
B
PSMB1v
PrS-SpeMreB1
PrS-SpeMreB4
Monomeric PrS-SpeMreB1
A280 (mAU)
Log (molecular weight)
Elution volume (mL)
C
15 μM PrS-SpeMreB1
2 mM MgATP, 100 mM KCl
500 nm
D
15 μM PrS-SpeMreB1
2 mM MgATP, 500 mM KCl
300 nm
E
SpeMreB conct.
1 μM
2 μM
3 μM
Sup
Ppt
PrS-SpeMreB1 WT (+) 2 mM ATP
PrS-SpeMreB1 WT (−) ATP
5 μM
7 μM
9 μM
PrS-SpeMreB1 WT (+) 2 mM ADP
PrS-SpeMreB1 WT (+) 2 mM AMPPNP
PrS-SpeMreB1 T164A (+) 2 mM ATP
F
WT (+) ATP
T164A (+) ATP
WT (+) ADP
[Ppt] (μM)
[Total] (μM)
G
PrS-SpeMreB1 WT
PSMB1v WT
PrS-SpeMreB1 E275R
PrS-SpeMreB1 T164A
SpeMreB5 E271R
PrS
[Pi] (μM)
Time (s)
H
rate (nM / s)
MreB (μM)
I
E275 in SpeMreB1 /
E285 in SpeMreB3 /
E271 in SpeMreB5

Fig 2

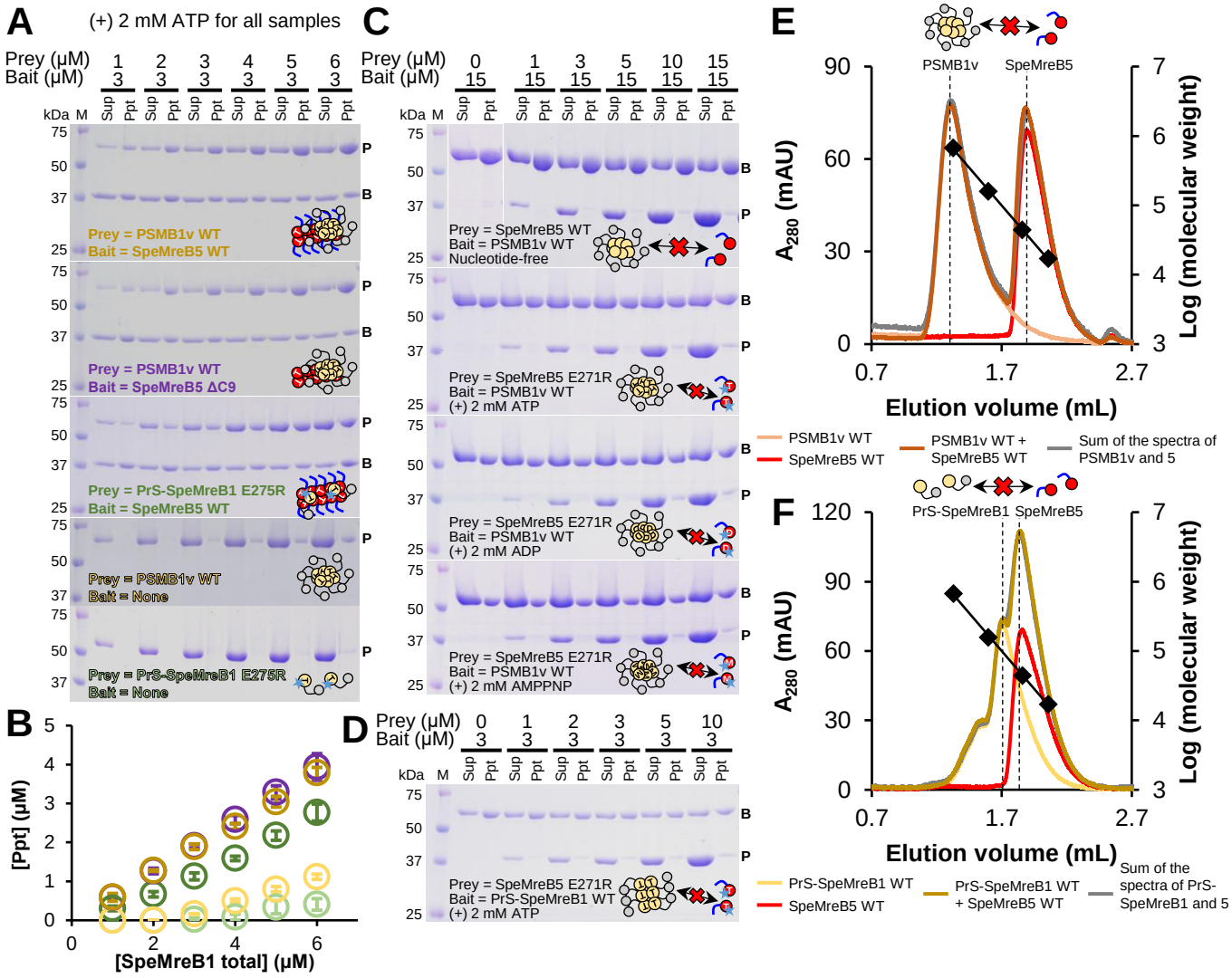
A
(+) 2 mM ATP for all samples
Prey (μM)
Bait (μM)
kDa M Sup Ppt
Prey = PSMB1v WT
Bait = SpeMreB5 WT
Prey = PSMB1v WT
Bait = SpeMreB5 ΔC9
Prey = PrS-SpeMreB1 E275R
Bait = SpeMreB5 WT
Prey = PSMB1v WT
Bait = None
Prey = PrS-SpeMreB1 E275R
Bait = None
P
B
[Ppt] (μM)
[SpeMreB1 total] (μM)
C
Prey = SpeMreB5 WT
Bait = PSMB1v WT
Nucleotide-free
Prey = SpeMreB5 E271R
Bait = PSMB1v WT
(+) 2 mM ATP
Prey = SpeMreB5 E271R
Bait = PSMB1v WT
(+) 2 mM ADP
Prey = SpeMreB5 E271R
Bait = PSMB1v WT
(+) 2 mM AMPPNP
D
Prey = SpeMreB5 E271R
Bait = PrS-SpeMreB1 WT
(+) 2 mM ATP
E
PSMB1v
SpeMreB5
A280 (mAU)
Log (molecular weight)
Elution volume (mL)
PSMB1v WT
SpeMreB5 WT
PSMB1v WT +
SpeMreB5 WT
Sum of the spectra of
PSMB1v and 5
F
PrS-SpeMreB1
SpeMreB5
PrS-SpeMreB1 WT
SpeMreB5 WT
PrS-SpeMreB1 WT
+ SpeMreB5 WT
Sum of the
spectra of PrS-
SpeMreB1 and 5

Fig 3

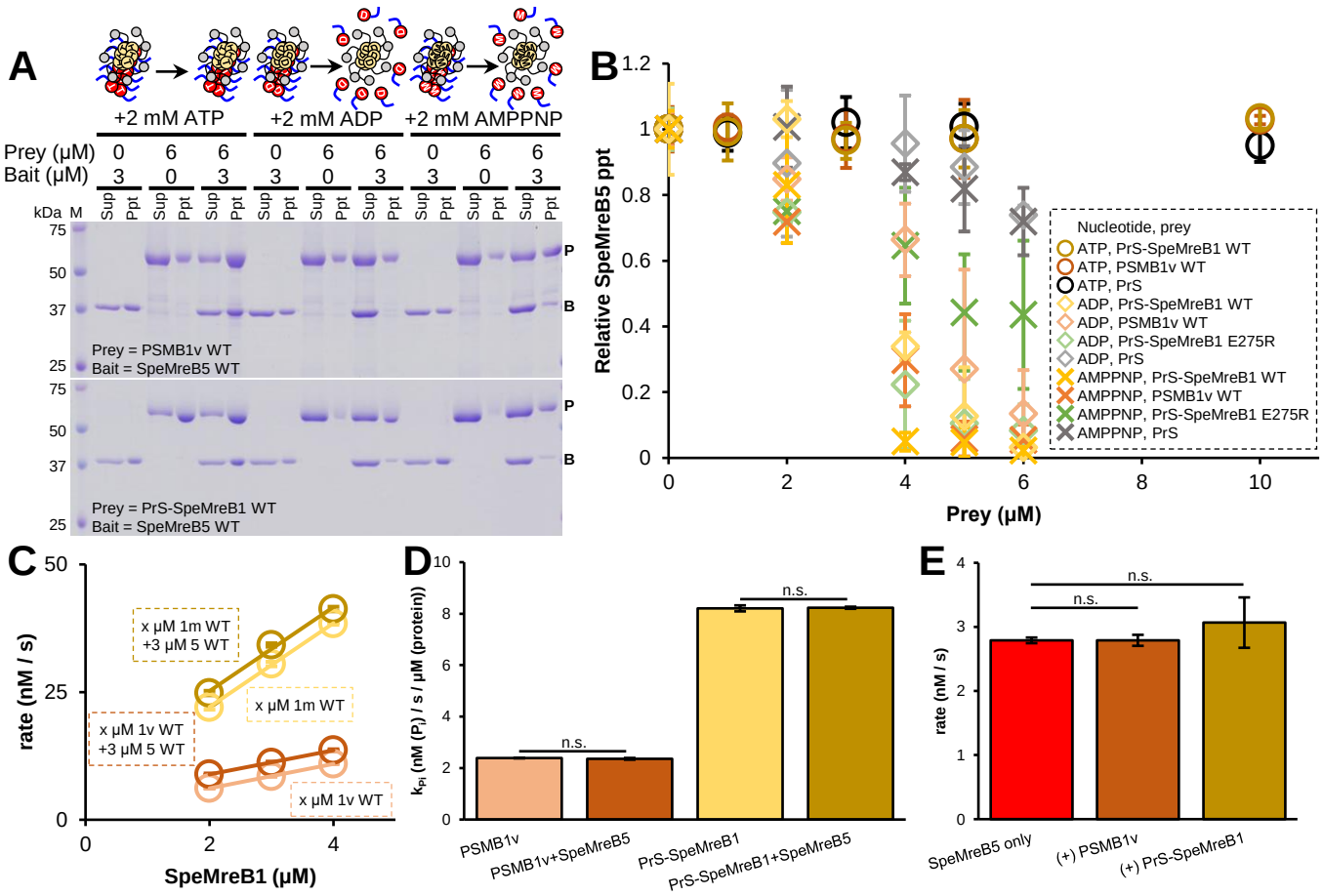
A
+2 mM ATP
+2 mM ADP
+2 mM AMPPNP
Prey (μM) 0 6 6 0 6 6 0 6 6
Bait (μM) 3 0 3 3 0 3 3 0 3
kDa M
Sup Ppt
75
50
37
25
P
B
Prey = PSMB1v WT
Bait = SpeMreB5 WT
Prey = PrS-SpeMreB1 WT
Bait = SpeMreB5 WT
B
Relative SpeMreB5 ppt
Prey (μM)
Nucleotide, prey
ATP, PrS-SpeMreB1 WT
ATP, PSMB1v WT
ATP, PrS
ADP, PrS-SpeMreB1 WT
ADP, PSMB1v WT
ADP, PrS-SpeMreB1 E275R
ADP, PrS
AMPPNP, PrS-SpeMreB1 WT
AMPPNP, PSMB1v WT
AMPPNP, PrS-SpeMreB1 E275R
AMPPNP, PrS
C
rate (nM / s)
SpeMreB1 (μM)
x μM 1m WT
+3 μM 5 WT
x μM 1m WT
x μM 1v WT
+3 μM 5 WT
x μM 1v WT
D
n.s.
PSMB1v
PSMB1v+SpeMreB5
PrS-SpeMreB1
PrS-SpeMreB1+SpeMreB5
E
n.s.
rate (nM / s)
SpeMreB5 only
(+) PSMB1v
(+) PrS-SpeMreB1

Fig 4

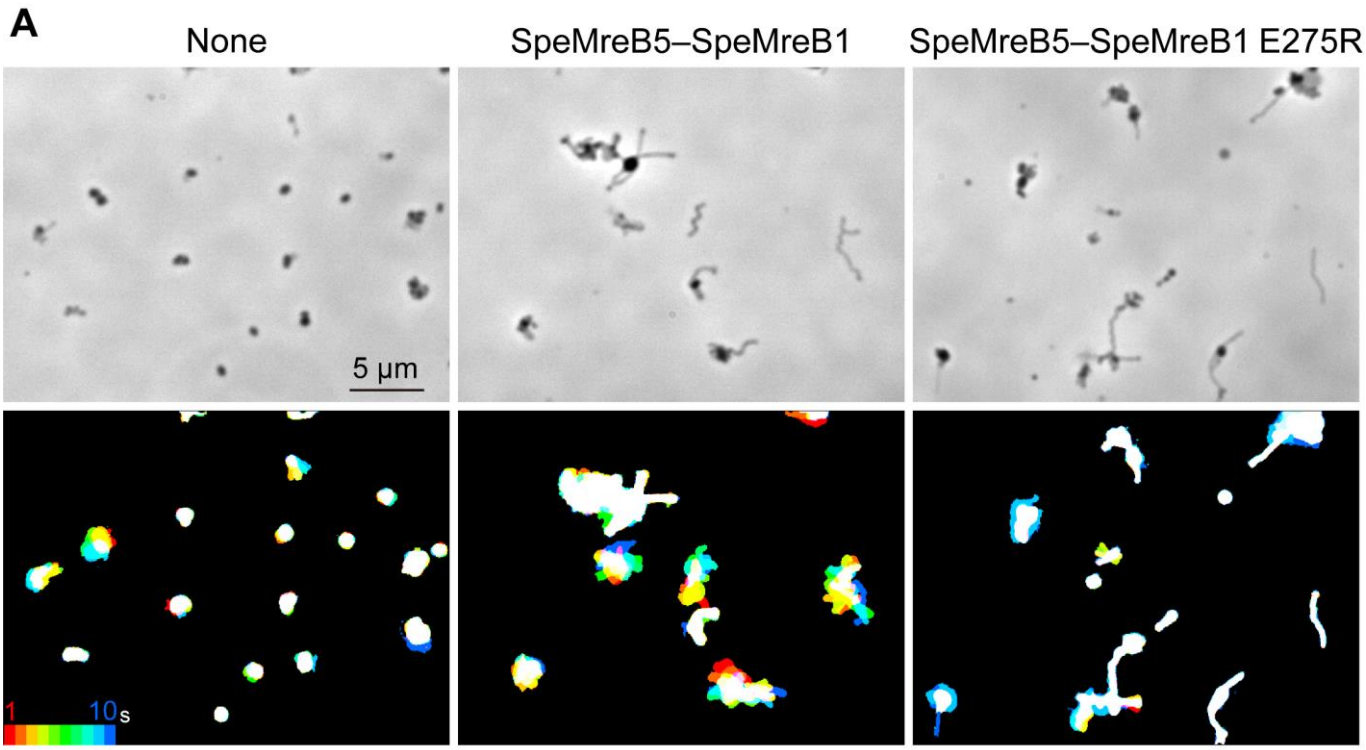
A
None
SpeMreB5–SpeMreB1
SpeMreB5–SpeMreB1 E275R
5 μm
1
10s

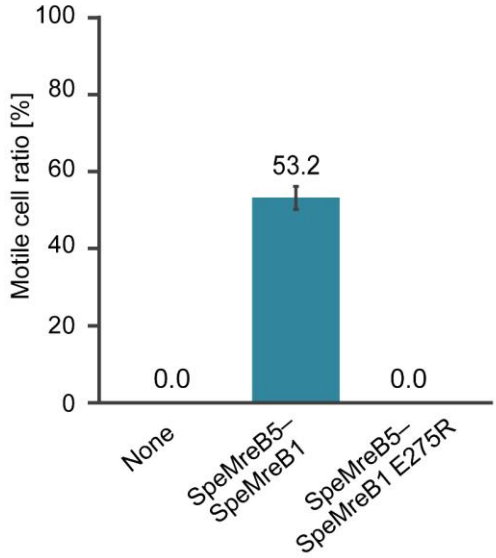
B
Motile cell ratio [%]
100
80
60
40
20
0
53.2
0.0
0.0
None
SpeMreB5–SpeMreB1
SpeMreB5–SpeMreB1 E275R

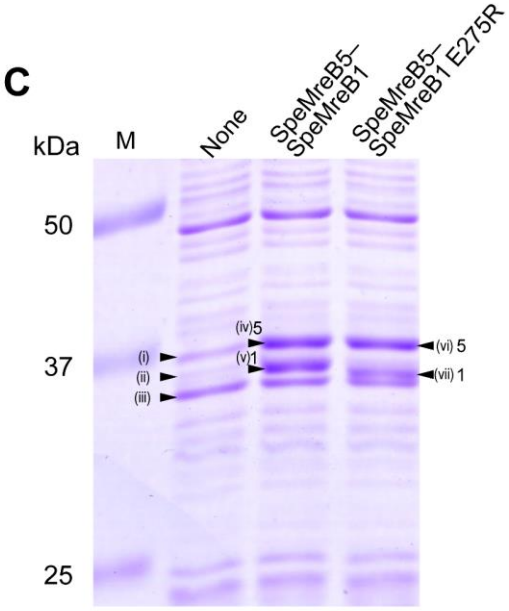
C
kDa
M
None
SpeMreB5–SpeMreB1
SpeMreB5–SpeMreB1 E275R
50
37
25
(i)
(ii)
(iii)
(iv) 5
(v) 1
(vi) 5
(vii) 1

Fig 5

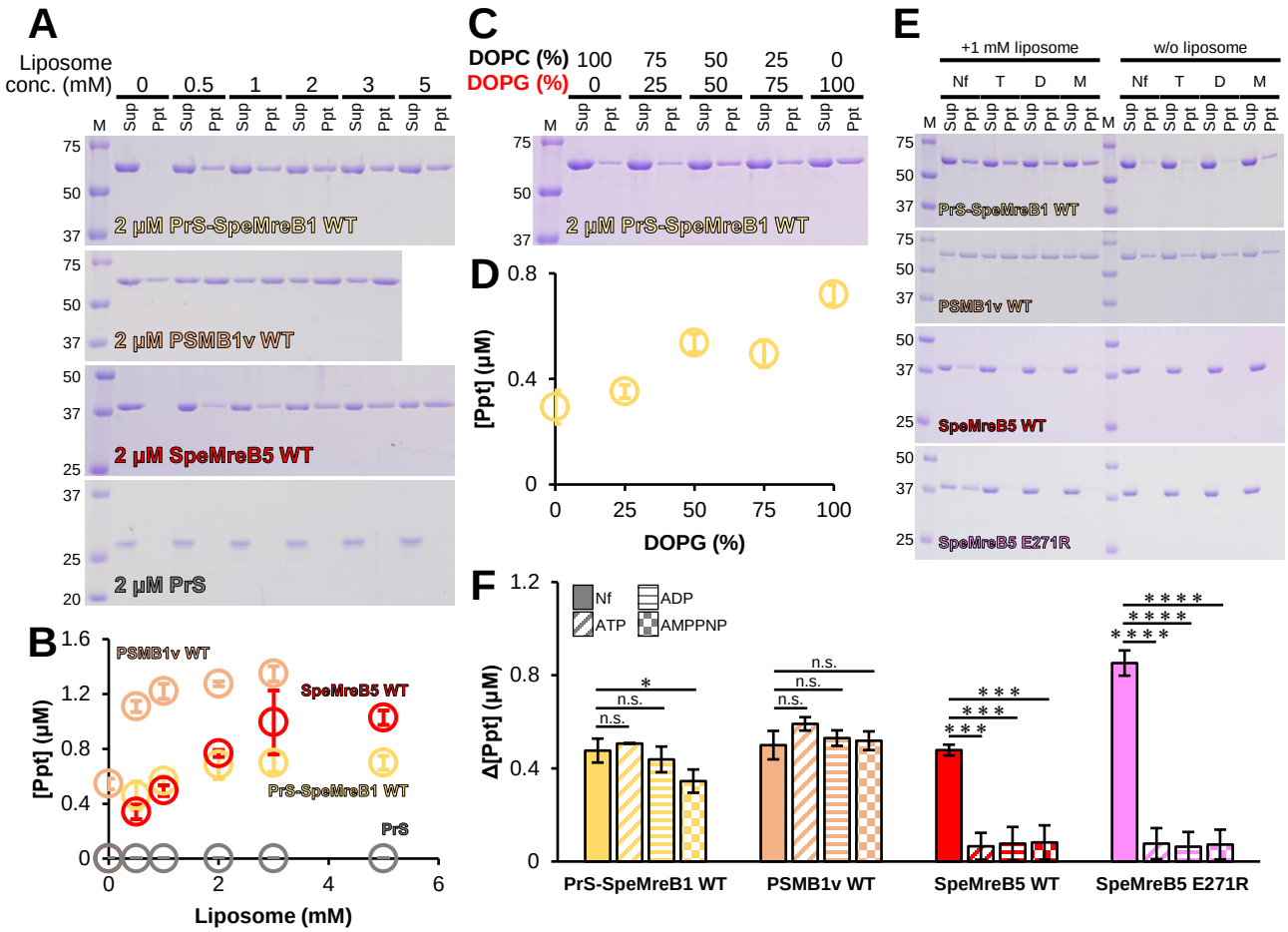
A
Liposome conc. (mM)
0
0.5
1
2
3
5
M
Sup
Ppt
2 μM PrS-SpeMreB1 WT
2 μM PSMB1v WT
2 μM SpeMreB5 WT
2 μM PrS
B
[Ppt] (μM)
Liposome (mM)
PSMB1v WT
SpeMreB5 WT
PrS-SpeMreB1 WT
PrS
C
DOPC (%) 100 75 50 25 0
DOPG (%) 0 25 50 75 100
D
[Ppt] (μM)
DOPG (%)
E
+1 mM liposome
w/o liposome
Nf
T
D
M
PrS-SpeMreB1 WT
PSMB1v WT
SpeMreB5 WT
SpeMreB5 E271R
F
Nf
ATP
ADP
AMPPNP
Δ[Ppt] (μM)
n.s.
PrS-SpeMreB1 WT
PSMB1v WT
SpeMreB5 WT
SpeMreB5 E271R

Fig 6

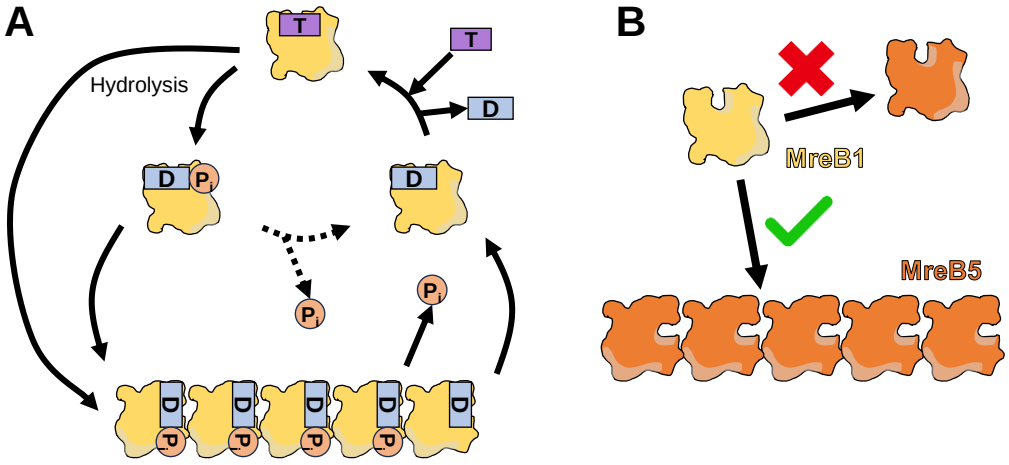

Fig S1

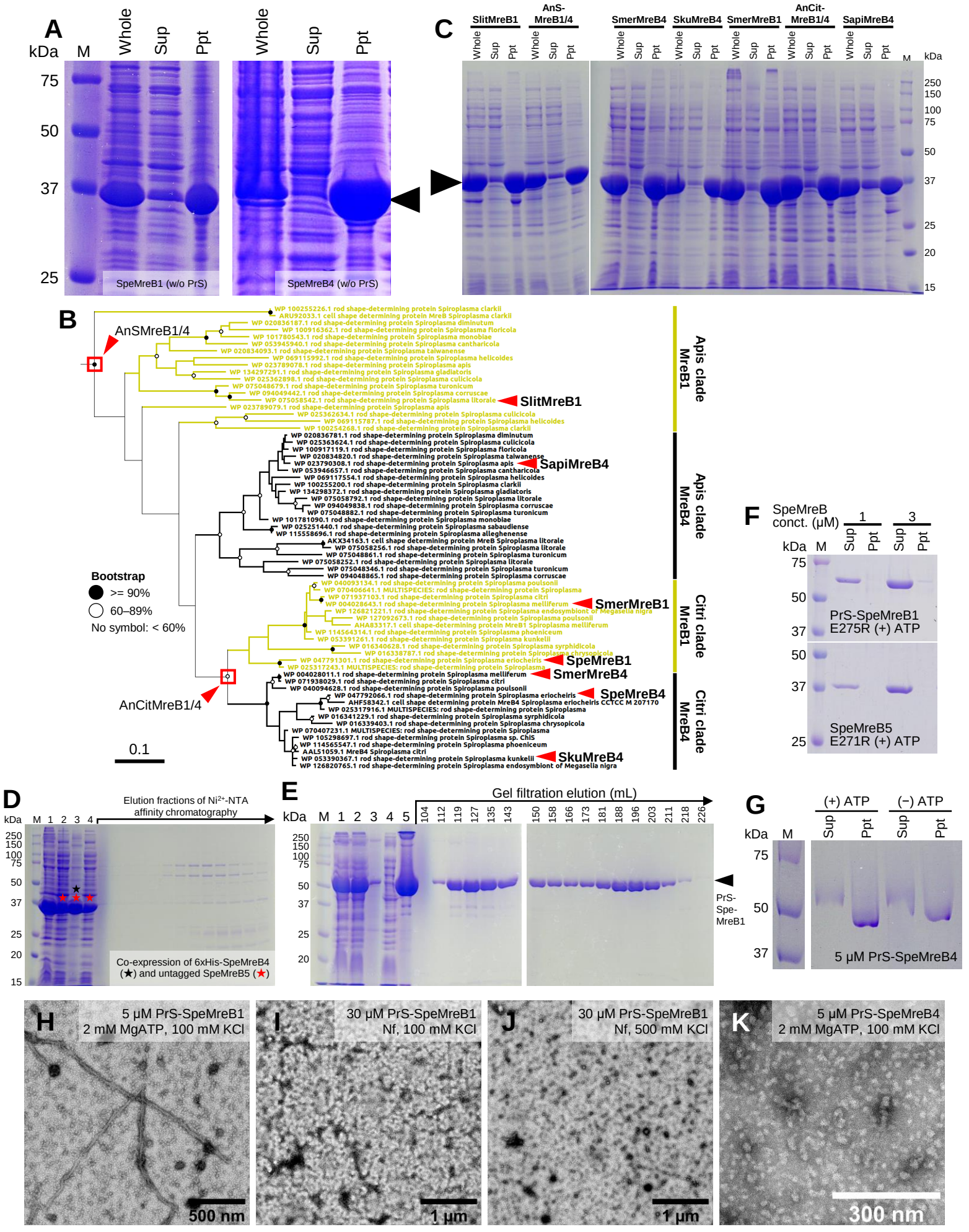
A
kDa
M
Whole
Sup
Ppt
75
50
37
25
SpeMreB1 (w/o PrS)
SpeMreB4 (w/o PrS)
C
SlitMreB1
AnS-MreB1/4
SmerMreB4
SkuMreB4
SmerMreB1
AnCit-MreB1/4
SapiMreB4
250
150
100
75
50
37
25
20
15
B
AnSMreB1/4
AnCitMreB1/4
SlitMreB1
SapiMreB4
SmerMreB1
SpeMreB1
SmerMreB4
SpeMreB4
SkuMreB4
Apis clade MreB1
Apis clade MreB4
Citri clade MreB1
Citri clade MreB4
Bootstrap
>= 90%
60–89%
No symbol: < 60%
0.1
F
SpeMreB conct. (μM)
1
3
Sup
Ppt
PrS-SpeMreB1 E275R (+) ATP
SpeMreB5 E271R (+) ATP
D
Elution fractions of Ni2+-NTA affinity chromatography
M 1 2 3 4
Co-expression of 6xHis-SpeMreB4 (★) and untagged SpeMreB5 (★)
E
Gel filtration elution (mL)
M 1 2 3 4 5
104 112 119 127 135 143 150 158 166 173 181 188 196 203 211 218 226
PrS-Spe-MreB1
G
(+) ATP
(−) ATP
Sup
Ppt
5 μM PrS-SpeMreB4
H
5 μM PrS-SpeMreB1
2 mM MgATP, 100 mM KCl
500 nm
I
30 μM PrS-SpeMreB1
Nf, 100 mM KCl
1 μm
J
30 μM PrS-SpeMreB1
Nf, 500 mM KCl
1 μm
K
5 μM PrS-SpeMreB4
2 mM MgATP, 100 mM KCl
300 nm

Fig S2

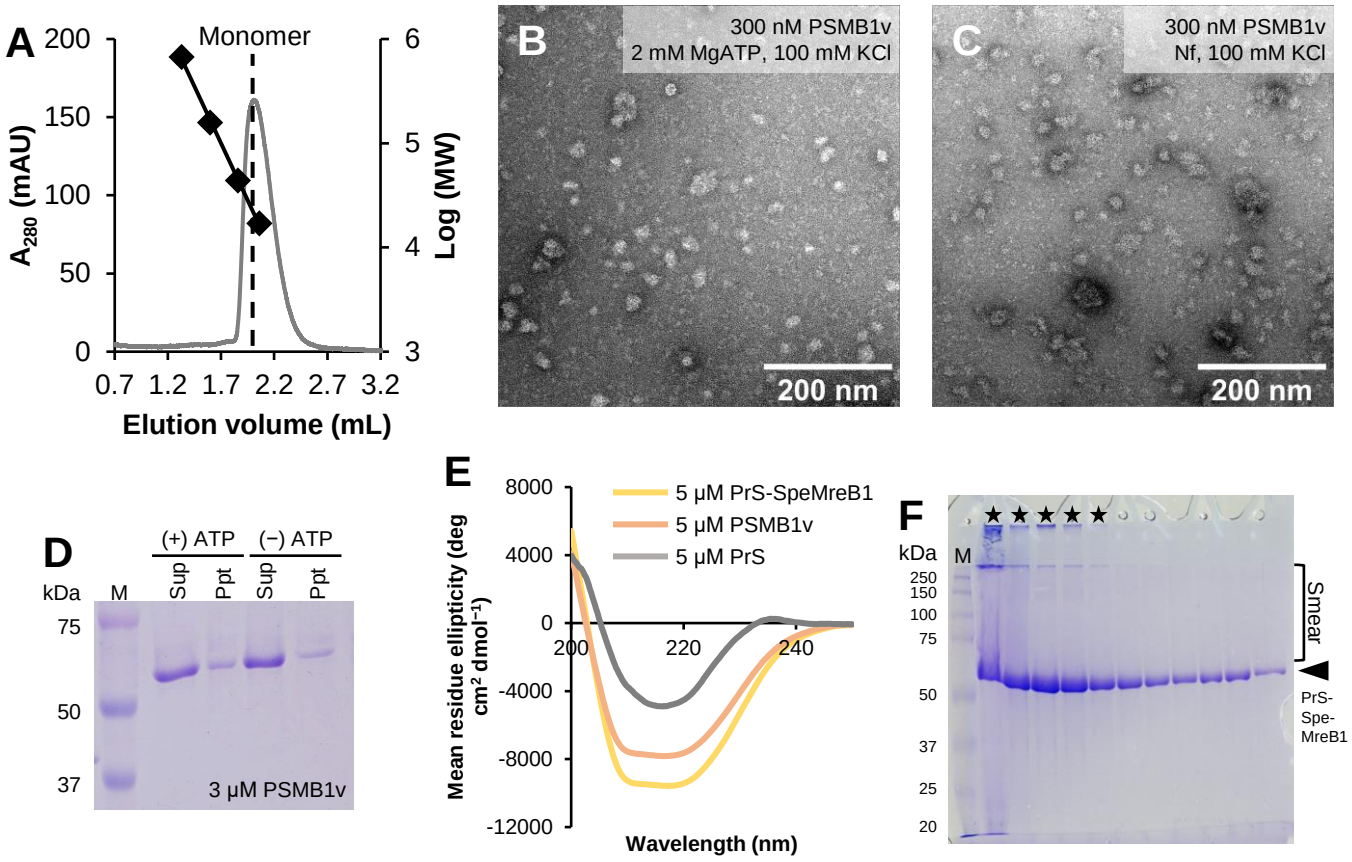
A
Monomer
A_{280} (mAU)
Log (MW)
Elution volume (mL)
B
300 nM PSMB1v
2 mM MgATP, 100 mM KCl
200 nm
C
300 nM PSMB1v
Nf, 100 mM KCl
200 nm
D
(+) ATP
(−) ATP
kDa
M
Sup
Ppt
Sup
Ppt
3 μM PSMB1v
E
5 μM PrS-SpeMreB1
5 μM PSMB1v
5 μM PrS
Mean residue ellipticity (deg cm² dmol⁻¹)
Wavelength (nm)
F
kDa
M
Smear
PrS-Spe-MreB1

Fig S3

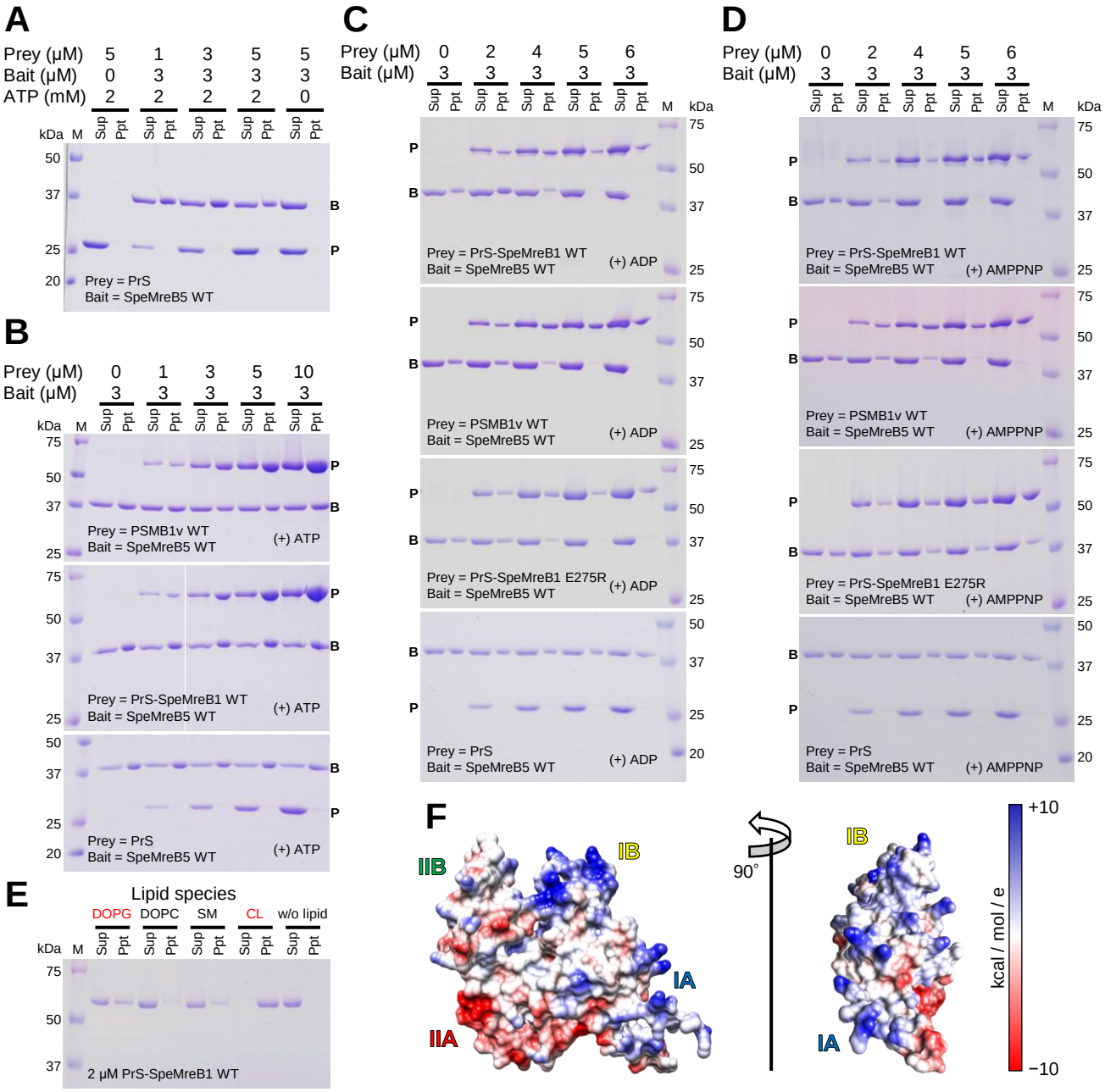
A
Prey (μM) 5 1 3 5 5
Bait (μM) 0 3 3 3 3
ATP (mM) 2 2 2 2 0
Sup Ppt
kDa M
50
37
25
20
B
P
Prey = PrS
Bait = SpeMreB5 WT
B
Prey (μM) 0 1 3 5 10
Bait (μM) 3 3 3 3 3
75
Prey = PSMB1v WT
Bait = SpeMreB5 WT
(+) ATP
Prey = PrS-SpeMreB1 WT
Bait = SpeMreB5 WT
(+) ATP
Prey = PrS
Bait = SpeMreB5 WT
(+) ATP
E
Lipid species
DOPG DOPC SM CL w/o lipid
2 μM PrS-SpeMreB1 WT
C
Prey (μM) 0 2 4 5 6
Bait (μM) 3 3 3 3 3
Prey = PrS-SpeMreB1 WT
Bait = SpeMreB5 WT
(+) ADP
Prey = PSMB1v WT
Bait = SpeMreB5 WT
(+) ADP
Prey = PrS-SpeMreB1 E275R
Bait = SpeMreB5 WT
(+) ADP
Prey = PrS
Bait = SpeMreB5 WT
(+) ADP
D
Prey (μM) 0 2 4 5 6
Bait (μM) 3 3 3 3 3
Prey = PrS-SpeMreB1 WT
Bait = SpeMreB5 WT
(+) AMPPNP
Prey = PSMB1v WT
Bait = SpeMreB5 WT
(+) AMPPNP
Prey = PrS-SpeMreB1 E275R
Bait = SpeMreB5 WT
(+) AMPPNP
Prey = PrS
Bait = SpeMreB5 WT
(+) AMPPNP
F
IIB
IB
IA
IIA
90°
IB
IA
+10
kcal / mol / e
−10